



1 Evaluating the Consistency and Continuity of Pixel-Scale Cloud

2 Property Data Records From *Aqua* and *SNPP*

3 Qing Yue¹, Eric J. Fetzer¹, Likun Wang², Brian H. Kahn¹, Nadia Smith³, John Blaisdell⁴, Kerry

4 G. Meyer⁵, Mathias Schreier¹, Bjorn Lambrigtsen¹, and Irina Tkatcheva¹

5 ¹Jet Propulsion Laboratory, California Institute of Technology, Pasadena, CA

6 ²Earth System Science Interdisciplinary Center, University of Maryland, 5825 University Research Court, Suite 4001,
7 College Park, MD 20740.

8 ³Science and Technology Corporation, 10015 Old Columbia Road, Columbia, MD 21046

9 ⁴Science Applications International Corporation, 12010 Sunset Hills Road, Reston, VA 20190

10 ⁵NASA Goddard Space Flight Center, Greenbelt, MD.

11

12

13 Correspondence to: Qing Yue (qing.yue@jpl.nasa.gov)

14 Abstract

15 The *Aqua*, *SNPP*, and *JPSS* satellites carry a combination of hyperspectral infrared sounders
16 (AIRS, CrIS) and high-spatial-resolution narrowband imagers (MODIS, VIIRS). They provide an
17 opportunity to acquire high-quality long-term cloud data records and are a key component of the
18 existing Program of Record of cloud observations. By matching observations from sounders and
19 imagers across different platforms at pixel scale, this study evaluates the self-consistency and
20 continuity of cloud retrievals from *Aqua* and *SNPP* by multiple algorithms, including the AIRS
21 Version-7 retrieval algorithm and the Community Long-term Infrared Microwave Combined
22 Atmospheric Product System (CLIMCAPS) Version-2 for sounders, and the Standard *Aqua*-
23 MODIS Collection-6.1 and the NASA MODIS-VIIRS continuity cloud products for imagers.
24 Metrics describing detailed statistical distributions at sounder field of view (FOV) and the joint
25 histograms of cloud properties are evaluated. These products are found highly consistent despite
26 their retrieval from different sensors using different algorithms. Differences between the two
27 sounder cloud products are mainly due to cloud clearing and treatment of clouds in scenes with
28 unsuccessful atmospheric profile retrievals. The sounder subpixel cloud heterogeneity evaluated
29 using the standard deviation of imager retrievals at sounder FOV shows good agreement between
30 the standard and continuity products from different satellites. However, impact of algorithm and
31 instrument differences between MODIS and VIIRS is revealed in cloud top pressure retrievals and
32 in the imager cloud distribution skewness. Our study presents a unique aspect to examine NASA's
33 progress toward building a continuous cloud data record with sufficient quality to investigate
34 clouds' role in global environmental change.

35

36

37



38 1. Introduction

39 Clouds play an important role in Earth’s energy balance and hydrological cycle. They occur
40 with processes involving atmospheric radiation, thermodynamics, and dynamics at various spatial
41 and temporal scales, making clouds a crucial component of the weather and climate system. With
42 daily regional and global coverage, space observations provide a unique vantage point to monitor
43 the change of the cloud properties in the climate system across different time scales. This offers
44 an important observational basis to resolve cloud processes in the background atmospheric
45 circulation, which is widely recognized as a critical challenge within Earth Sciences (Bony et al.
46 2015, IPCC 2013). The 2017 US National Academy Decadal Survey (ESAS 2017) has noted the
47 importance of long-term and sustained observations of many key components of the Earth system,
48 including continuity measurements of clouds. Many of these observations are obtained from the
49 existing Program of Record (POR). Since the “POR forms the foundation upon which the
50 committee’s recommendations are established” (ESAS 2017), it is crucial to evaluate whether a
51 self-consistent and continuous POR for cloud-related variables is indeed available with sufficient
52 data quality and spatio-temporal coverage.

53 Cloud retrievals from the NASA’s Earth Observing System (EOS) satellites, including *Terra*
54 and *Aqua*, the joint NASA/NOAA Suomi National Polar-orbiting Partnership (*SNPP*), and
55 NOAA’s new generation of Joint Polar Satellite System (*JPSS*) series weather satellites, are a key
56 component in the POR for cloud properties. Through efforts on continuity and consistency by
57 rigorous instrument mission design and ongoing algorithm development, these satellites provide
58 high quality, long-term cloud data records derived from the Top of Atmosphere (TOA) radiances
59 observed across a wide range of the emission and reflection spectrum. Particularly, *Aqua*, *SNPP*,
60 and *JPSS-1* (now *NOAA-20*), which were launched in 2002, 2011, and 2016, respectively, carry



61 high spatial resolution narrowband imagers, hyperspectral infrared (IR) sounders, and microwave
62 (MW) sounding measurements. As a result, observations with similar spatial resolution and
63 coverage, and similar spectral resolution at analogous wavelengths are obtained from different
64 satellites. For *Aqua*, this instrument trio consists of the Atmospheric Infrared Sounder (AIRS), the
65 Advanced Microwave Sounding Unit (AMSU), and the Moderate Resolution Imaging
66 Spectroradiometer (MODIS). For *SNPP* and *JPSS*, the trio includes the Cross-track Infrared
67 Sounder (CrIS), the Advanced Technology Microwave Sounder (ATMS), and the Visible Infrared
68 Imaging Radiometer Suite (VIIRS).

69 Retrieval algorithms to maintain the continuity of the data records across these platforms have
70 been developed. For joint retrievals by IR and MW sounders such as AIRS/AMSU and
71 CrIS/ATMS, the Community Long-term Infrared Microwave Combined Atmospheric Product
72 System (CLIMCAPS; Smith and Barnet, 2019) provides cloud properties together with vertical
73 profiles of atmospheric temperature, water vapor, and trace gases, as well as surface conditions.
74 For imagers like MODIS and VIIRS, the NASA MODIS-VIIRS continuity cloud products have
75 been developed for both cloud mask (CLDMSK; Frey et al. 2020) and cloud optical properties
76 (CLDPROP; Platnick et al. 2021). These continuity algorithms have heritage with NASA
77 operational retrieval products previously developed for individual sensors and satellites, such as
78 the AIRS Science Team retrieval algorithm Version 7 (AIRS V7, Yue and Lambrigsten 2017, 2020)
79 in the case of CLIMCAPS, and the Standard *Terra/Aqua* MODIS Collection 6.1 cloud retrievals
80 (MOD35/MYD35, MOD06/MYD06; Baum et al. 2012, Platnick et al. 2017) in the case of
81 MODIS-VIIRS. However, significant differences exist between the standard and continuity
82 algorithms, as the focus of the continuity algorithms is to minimize the impact of instrument
83 between platforms.



84 The sounder-imager combination on the same sun-synchronous polar-orbiting satellite,
85 together with the temporal coverage overlap between satellites, provides opportunities to utilizing
86 spectral and spatial capabilities from different sensors at global scale. Previous studies have shown
87 the benefits of using the combined information to intercalibrate and test radiometric consistency
88 among sensors (Tobin et al. 2006, Schreier et al. 2010, Wong et al. 2015, Gong et al. 2018); cross-
89 validate the retrievals (Nasiri et al. 2011, Kahn et al. 2014); further improve atmospheric and
90 surface geophysical parameter retrievals (Irion et al. 2018, Yao et al. 2015); provide simultaneous
91 observations to resolve complex physical processes (Yue et al. 2013, 2016, 2019, McCoy et al.
92 2017); quantify the subpixel heterogeneity (Li et al. 2004, Kahn et al. 2015); and enhance the
93 utilization of satellite observations in numerical weather prediction and climate models (Eresmaa
94 2014). Therefore, the sounder-imager combination is an important aspect of data record continuity
95 and consistency among sensors across different platforms. This helps provide robust monitoring
96 of long-term changes in cloud properties, an important capability expected from the POR.

97 Pixel-scale analyses are an effective and unique way to investigate the consistency and
98 continuity of these data records because of the one-to-one relationships established by these
99 comparisons and their direct links to algorithm performance. This includes examining differences
100 of (1) the same physical parameters observed by different sensors or satellites but processed using
101 the same (or similar) algorithms, and (2) the same parameters obtained from the same sensor but
102 from different algorithms. Both of these differences are quantified at the pixel scale in this study.
103 The cloud properties determined by the sounder and imager pairs on board *Aqua* and *SNPP*,
104 namely AIRS/MODIS and CrIS/VIIRS, are investigated using the collocated sounder-imager
105 fields of view (FOVs) for sets of pixels obtained during Simultaneous Nadir Observations (SNOs)
106 between *Aqua*-AIRS and *SNPP*-CrIS. This approach ensures nearly identical viewing geometry



107 by the two satellites while pixel-scale cloud assessment is carried out by comparing cloud
108 parameters determined by hyperspectral IR sounders and high spatial resolution imagers at the
109 minimum spatial scale of individual instrument fields of view. Using this approach, products from
110 both the heritage NASA standard retrieval algorithms and the newly-developed continuity cloud
111 algorithms are analyzed (Table 1). This is essential for retrieval algorithm development and cross-
112 validation of multiple sensors and products on *Aqua* and *SNPP*, and also important for data
113 continuity extending to future *JPSS* satellites.

114

115 **2. Data and Methodology**

116 2.1 Cloud products and algorithms

117 Table 1 summarizes the cloud parameters analyzed in this study from various Level 2 (L2)
118 retrieval products derived from the sounders and imagers aboard *Aqua* and *SNPP*. For AIRS and
119 MODIS, both the standard operational and continuity products are evaluated: the AIRS V7 and
120 CLIMCAPS-*Aqua* Version 2 (V2) retrievals for AIRS, and the Collection 6.1 *Aqua* MODIS
121 Atmosphere Level 2 Cloud Product (MYD06) and Version 1.1 NASA *Aqua* MODIS Continuity
122 Cloud Property Products (CLDPROP_MODIS). For *SNPP*-CrIS and -VIIRS, only the continuity
123 products are evaluated, which are the V2 CLIMCAPS-*SNPP* and Version 1.1 *SNPP*-VIIRS
124 Continuity Cloud Property Products (CLDPROP_VIIRS). The CLIMCAPS-*SNPP* products were
125 produced using Version 2 of the CrIS Level-1B product in Nominal Spectral Resolution (NSR)
126 and Full Spectral Resolution (FSR), which differ in the spectral resolution of the shortwave and
127 mid-IR CrIS observations transmitted from *SNPP* (Monarrez et al. 2020). The spectral resolution
128 differences cause subtle differences between the CLIMCAPS FSR and NSR retrievals, especially
129 in the upper tropospheric humidity and trace gases (Wang et al. 2021).



130 In both the AIRS V7 and CLIMCAPS algorithms for AIRS and CrIS, the radiatively effective
131 cloud amount (effective cloud fraction, ECF) and cloud top pressure (CTP) are retrieved by
132 matching the calculated cloudy radiances with the observed radiances for a set of channels that are
133 sensitive to clouds. Then the cloud top temperature (CTT) is derived as the atmospheric
134 temperature matching the retrieved CTP. In this process, best estimates of surface and atmospheric
135 parameters are used to calculate the cloudy radiances, either from the *a priori* state or from the
136 physical retrieval after the cloud clearing step (Susskind et al. 2003, Susskind et al. 2006, Smith
137 and Barnet 2019). The cloud clearing approach (Chahine 1974) is applied in both the AIRS Science
138 Team algorithms and CLIMCAPS. It predicts a single cloud cleared radiance at one AMSU or
139 ATMS field of regard (FOR) using *a priori* temperature, water vapor, and surface information and
140 a linear combination of IR radiances from nine AIRS or CrIS FOVs that are co-registered with one
141 AMSU or ATMS FOR (Susskind et al. 2003). The cloud cleared radiances are subsequently used
142 to retrieve surface and atmospheric parameters. Flowcharts of the retrieval steps and differences
143 in these two sounder retrieval systems are given in Thrastarson et al. (2021).

144 The ECF is the product of cloud areal fraction and the IR cloud emissivity, the latter of which
145 is assumed to be spectrally flat in the retrieval of ECF (Susskind et al. 2003). Previous studies
146 show that the AIRS ECF is consistent with the cloud properties such as the cloud frequency and
147 cloud optical depth measured by CloudSat and MODIS (Yue et al. 2011, Kahn et al. 2014). The
148 AIRS and CrIS retrievals of ECF and cloud top properties (CTT and CTP) are reported for up to
149 two cloud layers in each IR sounder FOV (~13.5 km spatial resolution at nadir).

150 There are distinct differences between the AIRS V7 and CLIMCAPS V2 algorithms regarding
151 cloud retrievals, summarized here. The first major difference is how cloud clearing is iterated in
152 the retrieval flow. The second major algorithm difference is quality control (QC) procedures when



153 1) the physical retrieval of atmosphere and surface is not successful, and 2) the final-stage cloud
154 clearing is not successful (Susskind et al. 2014). The third major difference is the choice of the
155 prior states for the two algorithms. The AIRS Science Team algorithms, including both V6 and
156 V7, iterate cloud clearing multiple times, and cloud parameters are determined after the last
157 iteration of cloud clearing using the retrieved surface and atmospheric conditions (Fetzer et al.
158 2020). In contrast, CLIMCAPS V2 performs a single cloud clearing pass and cloud properties are
159 retrieved using the surface and atmospheric parameters from successful retrievals of surface and
160 atmospheric properties (Smith and Barnett 2019, Thrastarson et al. 2021). The QC procedure used
161 in the two sounder cloud retrievals are also different. AIRS V7 produces case-by-case QC
162 indicators for each retrieved variable; while CLIMCAPS V2 derives one QC value based on the
163 cloud clearing and retrieval status of temperature and water vapor, and the same QC value is
164 assigned to all retrieved variables for the given FOV, including the cloud parameters. Particularly,
165 in AIRS V7 cloud retrieval process, the final stage of cloud clearing and cloud retrievals uses the
166 surface and atmospheric variable retrievals, except for cases over ocean when the retrieved surface
167 temperature differs from the first guess by more than 5 K. For these cases, the surface temperature
168 and surface emissivity from the *a priori* are used instead, and cloud properties retrieved under this
169 condition are flagged as valid with QC=1, indicating successful cloud retrievals but potentially
170 higher uncertainty than QC=0. This surface test effectively filters out cases when the cloud top is
171 misidentified as surface and causes extremely small ECF values for overcast cloudy conditions
172 over ocean. For ~1% of cases the final cloud retrieval step does not complete successfully, and a
173 QC=2 flag is assigned to cloud parameters to indicate invalid retrievals. As a result, the AIRS V7
174 cloud retrievals produce a much higher percentage of cases with successful cloud retrievals (cloud
175 variable QC=0 or QC=1) than its temperature and water vapor profile products. For CLIMCAPS



176 V2, cloud clearing is not iterated and cloud parameters follow the QC procedure in the physical
177 atmospheric state retrievals. As a result, a much larger number of cases with QC=2 cloud retrievals
178 are reported by CLIMCAPS V2 compared to AIRS V7, especially for cloudier conditions or cases
179 with large cloud clearing errors, typically those FORs with low cloud contrast between associated
180 FOVs. Different *a priori* in the two retrieval systems impact their cloud retrievals. AIRS V7 uses
181 the Stochastic Cloud Clearing / Neural Network (SCCNN) solution as *a priori* on atmospheric
182 temperature and water vapor profiles and surface temperature trained using a few months of
183 European Center for Medium-Range Weather Forecasting (ECMWF) model analyses and
184 AIRS/AMSU radiances (Milstein and Blackwell 2016). For land and sea ice surface emissivity
185 prior estimates, AIRS V7 uses the University of Wisconsin – Madison Baseline Fit Emissivity
186 database (Seemann et al. 2008), which is based on the monthly climatology of MODIS land surface
187 emissivity product (MOD11) in 2008 (Thrastarson et al. 2021). The CLIMCAPS system (Smith
188 and Barnet 2020, Smith et al. 2021), instead, uses concurrent fields from the Version 2 Modern-
189 Era Retrospective analysis for Research and Application (MERRA-2, Gelaro et al. 2017) as the *a*
190 *priori* and implements the Combined ASTER (Advanced Spaceborne Thermal Emission and
191 Reflection Radiometer) and MODIS Emissivity database for land surface (Hook 2019). Over
192 ocean, both systems use the Masuda IR sea surface emissivity model (Masuda et al., 1988) as
193 modified by Wu and Smith (1997). Since the *a priori* temperature, water vapor, and surface
194 properties are used in the cloud clearing step, differences in the *a priori* contribute to the
195 differences between the retrieval products, including cloud properties (Yue and Lambriksen 2020,
196 Yue et al. 2021). Cloud clearing plays an important role in both retrieval systems, and physical
197 retrievals of surface and atmospheric parameters are obtained from the cloud cleared radiances,
198 which, in turn, impact the determination of cloud properties.



199 In addition to these major differences, the two sounder retrieval systems differ in the prior
200 estimates used for ECF and CTP. CLIMCAPS starts the cloud retrieval with background estimates
201 of 0.5 and 0.25 ECF at 350 hPa and 800 hPa CTP for the upper and lower cloud layers, respectively.
202 AIRS V7 uses 1/6 ECF at 350 hPa for the upper layer, and 1/3 ECF at 850 hPa (or 100 hPa above
203 surface in elevated terrain) for the lower cloud layer. However, since the final cloud retrievals of
204 both systems are shown to diverge significantly from their prior (Yue and Lambrigtsen 2020, Yue
205 et al. 2021), it is unlikely that different cloud prior estimates are a main contributor to the sounder
206 cloud retrieval product differences.

207 Although their spectral resolution is coarser than that of AIRS and CrIS, instruments like
208 MODIS and VIIRS provide high spatial-resolution cloud properties through information in
209 multiple narrowband channels covering the visible and IR spectral regions. However, significant
210 differences exist between the two imagers. MODIS measures the reflectance or radiance in 36
211 spectral bands, while VIIRS has an analogous subset of these bands (20 channels) plus a day/night
212 visible channel (Oudrari et al. 2015). The lack of near-IR and IR water vapor and CO₂ absorption
213 channels in VIIRS has important implications on the available information content for clouds with
214 respect to MODIS. This impacts the determination of clouds, especially the detection of multi-
215 layer clouds and clear sky in polar night conditions, and the determination of cloud thermodynamic
216 phase. It also impacts the retrieval of cloud-top properties, especially for high thin clouds.
217 Moreover, the difference of spectral location of the VIIRS 2.25 μm channel compared to the
218 analogous 2.13 μm MODIS channel has implications on the retrievals of cloud particle size, optical
219 depth, and thermodynamic phase (Platnick et al. 2020). On the other hand, VIIRS provides a higher
220 spatial resolution of 750 m at nadir in cloud property retrievals, compared to the 1-km resolution
221 in the Collection 6.1 MYD06 and cloud mask products. In addition, VIIRS has an onboard detector



222 aggregation scheme that limits the across-swath pixel growth. VIIRS edge of scan pixel size is
223 roughly 1.625 km x 1.625 km versus roughly 2km x 4.9 km for MODIS (Platnick et al. 2021). The
224 MYD06 products have been shown to provide stable and well characterized cloud data records
225 since 2002 (e.g. Yue et al. 2017). Given these instrument differences between MODIS and VIIRS,
226 and a need to develop a continuous data record extending beyond the MODIS era, the MODIS-
227 VIIRS CLDMSK cloud mask (Frey et al. 2020) and CLDPROP cloud-top and optical property
228 (Platnick et al. 2021) continuity algorithms were developed. By applying common algorithms to a
229 subset of channels available on both instruments, the continuity algorithms accommodate the
230 detailed channel differences between the two instruments while maximizing the information
231 content on cloud parameters.

232 The continuity CLDPROP products have direct heritage with the Collection 6.1 MODIS
233 atmosphere cloud retrievals (MYD06), with cloud-top property datasets provided by the CLOUDS
234 from AVHRR (the Advanced Very High Resolution Radiometer) - Extended (CLAVR-x)
235 processing system (Heidinger et al. 2012, 2014). CLAVR-x produces cloud phase reported as
236 Cloud_Phase_Cloud_Top_Properties in the MODIS-VIIRS continuity cloud products. It replaces
237 the MODIS CO₂ slicing solution for cloud top pressure retrievals for cold clouds with an IR-
238 window channel optimal estimation approach coupled with a Cloud-Aerosol Lidar and Infrared
239 Pathfinder Satellite Observations (CALIPSO)-derived *a priori*. As a result, the CLDPROP optical
240 property cloud phase algorithm (reported as Cloud_Phase_Optical_Properties) removes the
241 dependence on the cloud top solution method in MYD06. Differences in the look-up tables (LUT)
242 of spectral liquid cloud reflectance result in changes of effective particle size (Re) (Platnick et al.
243 2020) that, along with cloud optical depth (COD), are used to derive cloud water path. Differences
244 with the Collection 6.1 MODIS cloud retrieval algorithms, as well as inter-sensor differences



245 between MODIS and VIIRS, have been reported in detail in recent studies such as Frey et al. (2020)
246 and Platnick et al. (2021), which are based on granule comparisons and long-term mean statistics.
247

248 2.2 Simultaneous Nadir Observations (SNOs) of collocated satellites

249 The pixel-scale comparisons will use SNOs between *Aqua*-AIRS and *SNPP*-CrIS. These SNOs
250 contain pixel pairs of observations from the two instruments when they observe the same location
251 at approximately the same scan angle and time. The AIRS-CrIS SNOs used herein were originally
252 developed by the JPL Sounder Science Investigator Processing System (SIPS) for inter-calibration
253 of two sounders (Manning and Aumann 2015). In order to ensure a close match between the
254 instruments, the following criteria are used to identify candidate SNOs:

- 255 • FOV centers between *Aqua*-AIRS and *SNPP*-CrIS are within 8 km;
- 256 • Observations are made within 10 minutes;
- 257 • Both instruments observe within 3.3° of nadir, which corresponds with ± 1 FOR
258 of AMSU for AIRS or ATMS for CrIS.

259

260 2.3 Pixel-scale collocations of imagers and sounders:

261 Utilizing the multi-sensor capability at the pixel scale requires accurate and computationally
262 efficient collocation of sounder and imager measurements. Various collocation methods exist
263 (Schreier et al. 2010, Nagle and Holz 2009, Yue et al. 2013). In this study, the method developed
264 by Wang et al. (2016) is applied by matching the instantaneous multi-sensor observations directly
265 based on line-of-sight (LOS) pointing vectors, defined as the vector from the satellite position to
266 the Earth surface pixel location. The details of this method and its accuracy are discussed at length
267 in Wang et al. (2016).



268 In this study, the same collocation method is applied to both *Aqua* and *SNPP* to match the finer
269 resolution imager pixels (MODIS and VIIRS) within a given sounder FOV (AIRS and CrIS). The
270 LOS vectors are calculated using the geolocation datasets for different sensors, which contain
271 latitude, longitude, satellite range, satellite azimuth and zenith angles. Collocation is performed
272 using the criterion that the angular difference between the LOS vectors for sounder and imager
273 should be less than half of the sounder FOV size angle. The CrIS FOV is treated as a 0.963° circle
274 which corresponds to $\sim 41\%$ of the peak response and collects $\sim 98\%$ of total radiation falling on
275 the detector (Wang et al. 2013). AIRS has a FOV half-power width of 1.1° (Fishbein et al. 2001).
276 However, 0.963° is used for both AIRS and CrIS in the collocation. After obtaining collocation
277 indices, the L2 cloud properties from both the imagers and sounders are populated accordingly.
278 The high spatial resolution information from MODIS and VIIRS is retained using higher statistical
279 moments and frequency distributions of cloud properties retrieved by imagers within collocated
280 sounder FOV. These statistical metrics include the mean, standard deviation, skewness and
281 kurtosis of MODIS and VIIRS cloud properties, the occurrence frequency of cloud types and cloud
282 phase reported by the cloud mask and cloud thermodynamic phase variables, and joint histograms
283 on the COD and CTP two-dimensional space following the convention of the International Satellite
284 Cloud Climatology Project (ISCCP, Rossow and Schiffer 1999). In addition to summarizing fine
285 imager spatial information over a coarser resolution sounder instrument, these statistical metrics
286 physically describe a variety of cloud processes at both regional and global scales for a range of
287 cloud types in different climate regimes, which are particularly relevant to sub-grid cloud
288 parameterization in numerical models (e.g. Zhu and Zuidema 2009, Kawai and Teixeira 2010 and
289 2012, Kahn et al. 2017). The ISCCP-type of joint histograms have been widely used to dissect the



290 uncertainty of the cloud radiative forcing (e.g. Pincus et al. 2012) and climate feedback (e.g.
291 Zelinka et al. 2012, Yue et al. 2016 and 2019) by cloud regimes (e.g. Oreopoulos et al. 2016).

292 By combining the SNOs and the sounder-imager collocated datasets, a multi-sensor multi-
293 satellite investigation is conducted to evaluate, at pixel scale, the self-consistency of cloud
294 properties, to benchmark data continuity from the US polar-orbiting operational environmental
295 satellites.

296

297 **3. Results**

298 Both *Aqua* and *SNPP* are in the 1:30 PM local equatorial crossing time sun-synchronous polar
299 orbits, but at different altitudes. This altitude difference gives a ~ 2.667 day repeating pattern for
300 AIRS and *SNPP*-CrIS observations at the same location. Accordingly, the number of SNOs
301 between these two IR sensors varies with time and a large fraction are located at the high latitudes.
302 In this study, seven focus days in January 2016 are selected for their large numbers of SNO pairs
303 and the full operation for all four instruments. Table 2 lists the focus days and gives the number of
304 observations obtained on each day. Figure 1 shows the latitudinal distribution of the focus day
305 SNOs (black bars, y-axis on the left, Table 2). A significant number of observations ($>2,500$) are
306 available at all latitudes, including the midlatitudes and tropics where SNOs are harder to obtain.

307 Fig. 2 shows the latitudinal variations of cloud frequency and zonal mean ECF and COD based
308 on the data from the seven focus days. To determine the detection of clouds in the sounder FOV,
309 two threshold values of ECF are used: 0.05 (solid lines) and 0.01 (dash lines). For MODIS and
310 VIIRS, frequency of Cloudy, Uncertain cases as reported by the cloud mask variable is shown for
311 MYD06 (black), MODIS continuity (red), and VIIRS continuity (blue) cloud products. Although
312 it is difficult to directly compare the mean cloud properties retrieved by imagers and sounders,



313 AIRS V7 produces similar general patterns of latitudinal variation of cloud frequency with the
314 imager products, which shows peaks of cloud occurrence in the tropics and midlatitude storm
315 tracks, and troughs in the subtropics. However, CLIMCAPS V2 cloud retrievals do not show these
316 variations, and its mean ECF values are much lower than AIRS V7 at all latitudes. A higher
317 percentage of cloud frequency in the low latitude regions is reported by AIRS V7 than by imagers,
318 consistent with previous findings showing higher sensitivity of hyperspectral IR sounders to
319 optically thin clouds (Kahn et al. 2014, Yue et al. 2016). An increase of COD with latitude at mid
320 to high latitude regions is detected by imagers, compared to a nearly flat or even decreasing mean
321 ECF retrieved by the sounders. These differences will be further assessed in the following
322 discussions.

323

324 3.1 Clouds retrieved by hyperspectral IR sounders

325 In Fig. 1, overlapped with the SNO count histograms are the occurrence frequency of
326 sounder FOVs (colored lines, y-axis on the right) for four composites that satisfy the following
327 four conditions, respectively: $ECF > 0.01$ (general cloudy condition), $ECF \leq 0.01$ (clear or very
328 thin clouds), $ECF > 0.8$ (overcast or very thick clouds), and cases with successful CTP retrievals
329 (QC for CTP is 0 or 1). These ECF values are selected based on the relationships between clouds
330 and the IR sounder spectral information, as well as the retrieval uncertainty. The fraction of the
331 highest quality atmospheric state retrievals below clouds, obtained from IR spectral information,
332 decreases with higher ECF (Fetzer et al. 2006). The combination of IR and MW radiances can
333 facilitate the retrieval of vertically resolved temperature and humidity profiles up to ECF of
334 0.7~0.8 (Yue et al. 2011, Yue and Lambrigtsen 2020, Yue et al. 2021). The ECF of 0.01 is often
335 used as the threshold of cloud detection by IR sounders (e.g. Kahn et al. 2014). Moreover, it has



336 been shown that AIRS V7 cloud retrievals present higher uncertainty on thin, broken clouds and
337 cloud edges when $ECF < 0.01$ (Yue and Lambrigtsen 2020).

338 For each composite, the occurrence frequency is calculated as the percentage of AIRS or
339 CrIS FOVs with successful cloud retrievals that satisfy the composite condition relative to the
340 total number of FOVs in each latitudinal bin. The QC flags for each cloud parameter are reported
341 in the L2 products and used to determine whether the algorithm reports a successful cloud
342 retrieval (when $QC = 0$ or 1). Different colors are used to indicate retrieval algorithms for the
343 two sounders. Since AIRS V7 and CLIMCAPS retrieve cloud properties up to two cloud layers
344 over each IR sounder FOV, an effective CTP is calculated as the weighted mean CTP by the
345 ECF reported at each cloud layer.

346 These results show large differences between the AIRS V7 clouds with those from CLIMCAPS.
347 AIRS V7 produces a much larger number of cloudy observations (solid pink line in Fig. 1) and a
348 higher yield for CTP retrievals (dash dotted line, Fig. 1), except in the Antarctic region. The
349 magnitude of this difference reaches up to 30% over the Southern Hemisphere and the tropics.
350 Furthermore, AIRS V7 produces much more overcast or very thick clouds (dash lines, Fig. 1) but
351 fewer clear or very thin cloudy cases (dotted lines, Fig. 1) than CLIMCAPS, which is consistent
352 with smaller mean ECF and lower cloud frequency in the tropics and midlatitude storm track
353 regions by CLIMCAPS V2 in Fig. 2. As discussed previously, this is related to the differences
354 between the two algorithms for AIRS in cloud clearing and cloud retrieval QC, as well as the use
355 of different *a priori*. These differences are further evaluated in the following sections using the
356 imager observations.

357 Despite the differences of sensors, satellites, and spectral resolutions, the three CLIMCAPS
358 Version 2 retrievals evaluated in this study present similar latitudinal distributions of the cloud



359 property distribution and cloud detection. As seen from Fig. 1, CLIMCAPS-*Aqua* (green dotted
360 line) reports a higher percentage of clear or very thin cloudy cases than those for *SNPP* (yellow
361 dotted line for CLIMCAPS-*SNPP* FSR and purple for CLIMCAPS-*SNPP* NSR), especially in the
362 midlatitude region. Among the three CLIMCAPS products, CLIMCAPS-*Aqua* (green solid line)
363 reports fewer cloudy cases than CLIMCAPS-*SNPP* (yellow and purple solid lines) in midlatitudes,
364 but more cloudy cases in the tropics. The finer spectral resolution for CLIMCAPS-*SNPP* FSR
365 retrievals produces a higher percentage of cloudy FOVs than the coarser spectral resolution
366 radiances used by the NSR retrieval.

367 Figure 3 further characterizes the four IR sounder cloud retrievals using the joint distributions
368 of observations among different algorithms. It is known that larger uncertainty of both sounder
369 and imager retrievals exists over snow and ice covered surfaces (Chan and Comiso, 2013, Yue and
370 Lambrigtsen 2020), so in this comparison the data points located in regions poleward of 60° are
371 excluded. Cases are only included if both data products in the comparison (indicated by x- and y-
372 axes of the plot) report valid retrievals. The three CLIMCAPS retrievals (x-axes) are compared
373 with AIRS V7 (y-axes) for both ECF and CTP. The generally good agreement among the
374 algorithms and sensors, especially for CTP, is encouraging, which shows the robustness of these
375 products and consistency of information for clouds in hyperspectral IR sounders. However,
376 CLIMCAPS reports a large number of cases with ECFs between 0 and 0.1, for which AIRS V7
377 reports ECFs ranging from 0 (clear sky) and 1 (completely cloudy). This issue is further illustrated
378 in Fig. 4. For cases where CLIMCAPS-*Aqua* V2 retrieved ECF is less than 0.1, AIRS V7 (the
379 magenta line) shows two peaks in the ECF occurrence frequency. The first peak is located at V7
380 $ECF < 0.1$, indicating the two algorithms agree with each other in cloud amount detection. The
381 larger second peak shows that more than 25% of cases with CLIMCAPS $ECF < 0.1$ have AIRS



382 V7 ECF values of 0.8~0.9. As a result, the correlation coefficient (r) between ECF retrievals from
383 AIRS V7 and CLIMCAPS V2 is only 0.27, which increases to 0.79 when neglecting ECF < 0.1
384 observations.

385 A tighter agreement between CLIMCAPS V2 and AIRS V7 is seen for CTP retrievals as shown
386 by points densely located along the identity line in Fig. 3. The correlation coefficients between
387 CLIMCAPS-Aqua and AIRS V7 CTP are 0.69 for all cases and 0.92 for ECF > 0.1, respectively.
388 High cloud cases (AIRS V7 CTP < 440hPa) show a much higher CTP correlation ($r = 0.87$) than
389 for low clouds (AIRS V7 CTP > 600 hPa, $r = 0.43$). When both algorithms identify low clouds in
390 the FOV, CLIMCAPS reports a slightly lower cloud top (larger CTP) than AIRS V7, with a median
391 value difference of 12 hPa; whereas for high clouds, CLIMCAPS V2 reports a higher cloud top
392 with its median CTP 13 hPa smaller than the one by AIRS V7.

393 In the next section, these differences among the various sounder cloud retrieval products are
394 further evaluated using the cloud parameters determined by collocated MODIS and VIIRS data.
395

396 3.2 Comparison of sounder cloud properties and collocated imager measurements

397 Figures 5 and 6 compare the cloud properties retrieved from various sounder algorithms with
398 the collocated imager cloud retrievals in the MYD06 and CLDPROP_MODIS products,
399 respectively. Comparisons with CLDPROP_VIIRS are similar to those using CLDPROP_MODIS
400 and hence are not shown in these figures. The cloud properties from MODIS pixels are averaged
401 within the collocated sounder FOV before this comparison.

402 The IR sounder retrieved ECF is positively correlated with the imager observed COD in the
403 top rows of Figs. 5 and 6, showing the consistency of cloud amount determined using different
404 sensors. However, two main differences are noticed. First, it is clear that the CLIMCAPS V2 (for



405 both *Aqua* and *SNPP*) misidentifies a significant number of cloudy cases as clear or thin clouds.
406 As shown in Fig. 4, more than 50% of these cases are optically thick clouds with large cloud
407 amount ($ECF > 0.7$) reported by AIRS V7 and COD values ranging from 2 to 10 by MODIS and
408 VIIRS. Secondly, the comparisons between CLIMCAPS and imager cloud products do not have
409 the cluster corresponding to cases with both high ECF and large COD values, as in the comparison
410 between AIRS V7 and imagers. As discussed previously, this is related to misidentification of
411 cloudy cases as clear or thin cloud conditions by CLIMCAPS. However, another main cause is
412 that CLIMCAPS cloud retrievals have the same QC flags as the physical atmospheric state
413 retrievals; as a result, cases with large cloud amount are filtered out. In general, AIRS V7 products
414 exhibit better agreement with MODIS and VIIRS in detecting cloud amount and occurrence.
415 CLIMCAPS V2 cloud retrievals could be further improved with better cloud clearing flow and
416 more careful treatment when retrieving clouds with unsuccessful atmosphere physical retrievals.

417 The sounder and imager CTP retrievals are also compared in the bottom rows of Fig. 5 and 6.
418 Despite instrument and algorithm differences, when both sounder and imager detect high clouds
419 ($CTP < 440$ hPa, including $ECF < 0.1$ cases), CTP retrievals agree with each other well. The
420 correlation coefficients with MYD06 CTP are 0.77, 0.52, and 0.62 for AIRS V7, CLIMCAPS-
421 *Aqua*, and CLIMCAPS-*SNPP*-FSR, respectively. When imagers detect low clouds ($CTP > 680$
422 hPa), IR sounders determine the majority of cases as low clouds but with a tail toward CTP values
423 corresponding to high and mid-level clouds (middle row). The disagreement mainly occurs when
424 sounder retrieved ECF is less than 0.1 as shown by the magenta contour lines. These are cases
425 when larger uncertainty in infrared cloud retrieval exists, as discussed previously. After removing
426 these cases, the sounder-imager discrepancy in the low cloud conditions is reduced greatly (bottom
427 row), especially for AIRS V7. These differences are consistent with the known limitation of



428 imagers such as MODIS, which tend to miss high and thin cloud layers (Holz et al. 2008) when
429 compared with AIRS (Kahn et al. 2014). However, the analysis presented here cannot completely
430 rule out the impact of uncertainty in the IR sounder cloud retrievals. When both hyperspectral
431 sounders and narrowband imagers detect low clouds, sounders tend to retrieve smaller CTP than
432 imager. For AIRS V7, the median difference in this condition is -65, -77, and -80 hPa with MYD06,
433 CLDPROP_MODIS, and CLDPROP_VIIRS products, respectively.

434

435 3.3 Clouds retrieved by imagers

436 Figure 7 compares COD, CTP, and Re retrieved by different MODIS and VIIRS cloud
437 algorithms, with mean imager cloud properties over corresponding sounder FOVs are shown. Very
438 good agreement between MODIS and VIIRS, and between the MYD06 and continuity products is
439 seen. All correlation coefficients are greater than 0.8. For the three cloud parameters, correlation
440 is always the highest between products derived from the same instrument (MYD06 and
441 CLDPROP_MODIS), and the lowest between MYD06 and CLDPROP_VIIRS (but still reaching
442 0.81, 0.88, and 0.81 for COD, CTP, and Re, respectively) when both instrument and algorithm are
443 different. From the same instrument MODIS but different algorithms, the correlation is lowest for
444 CTP retrievals ($r = 0.89$) compared to COD ($r = 0.97$) and Re ($r = 0.97$). This is because MYD06
445 and the continuity cloud algorithm uses different methods and spectral channels to determine CTP.
446 However, a relationship near one-to-one is seen, indicating the consistency between the
447 operational and continuity cloud products from MODIS, at least for the cloud properties averaged
448 at the sounder resolution (~ 13.5 km). Correlations between MODIS and VIIRS cloud products are
449 lower than those from MODIS alone (with different algorithms), even when both products are
450 derived from the same continuity algorithm. The degradation of agreement is larger for COD and



451 Re than for CTP (Fig. 6). This reflects the effect of spectral channel and spatial resolution
452 differences between MODIS and VIIRS, as well as the related adjustments made to the continuity
453 algorithms, such as the liquid phase LUT for cloud microphysical retrievals. Another possible
454 factor is the collocation error existing in the SNOs, but this is ruled out since results with more
455 conservative collocation criteria remain largely the same (not shown).

456 To further analyze the differences between the imager cloud products and the subpixel cloud
457 heterogeneity over the sounder FOVs, the standard deviation and skewness of the imager cloud
458 property distributions over the sounder FOVs are shown in Fig. 8 and 9, respectively. Correlations
459 are weaker in these higher statistical moments, yet for standard deviation they remain larger than
460 0.6. Similar to comparisons for mean values, tight one-to-one relationships are seen for standard
461 deviation at the sounder FOV scale between the two MODIS cloud products. Similar to mean value
462 comparisons, the CTP standard deviation has the lowest correlation coefficient ($r = 0.63$) compared
463 to the ones for COD ($r = 0.96$) and Re ($r = 0.87$). However, skewness only shows significant
464 correlations for COD ($r = 0.78$) and Re ($r = 0.70$) between the two MODIS datasets, but poor
465 correlations ($r < 0.3$) for CTP. The impact from the differences in CTP algorithms thus shows up
466 more strongly on the higher statistical moments. When evaluating data from different sensors, no
467 correlation is seen for skewness of any of the cloud parameters even with the same retrieval
468 algorithms (Fig. 9, middle and right columns), different from the comparisons using mean value
469 and standard deviation (Figs. 7 and 8, middle and right columns).

470

471 3.4 Joint histograms, cloud types, and cloud thermodynamic phase

472 3.4.1 Cloud type by cloud property joint histograms



473 Figs. 10-13 show the two-dimensional cloud histograms calculated using SNOs from the focus
474 days over different surface types and regions, including the tropics ($30^{\circ}\text{N}\sim 30^{\circ}\text{S}$), over ocean (land
475 fraction < 0.1 , $60^{\circ}\text{N}\sim 60^{\circ}\text{S}$), over land (land fraction > 0.9 , $60^{\circ}\text{N}\sim 60^{\circ}\text{S}$), and over ice and snow
476 covered surfaces (frozen surfaces), respectively. The land fraction and surface classes are obtained
477 from the AIRS V7 L2 product under variable names of landFrac and SurfClass, respectively. For
478 MODIS and VIIRS, the ISCCP type of CTP-COD joint histograms are generated by summing the
479 joint distributions over individual AIRS and CrIS FOV, with no averaging over sounder FOV. For
480 AIRS and CrIS, joint distributions are calculated on the CTP and ECF space.

481 Consistent with results in previous sections, AIRS V7 shows peaks of both thin and thick
482 clouds while CLIMCAPS V2 products show a single peak distribution of thin clouds. Better
483 consistency of AIRS V7 with imager cloud products is also shown by the joint histograms. For
484 example, in the tropics (Fig. 10) clusters corresponding to optically thick high clouds, thin cirrus,
485 and broken or optically thin low clouds are seen in the AIRS V7 CTP-ECF histogram, consistent
486 with the patterns in the MODIS and VIIRS CTP-COD histograms. Agreement between AIRS V7
487 and imager clouds is also found for mid-level and low cloud clusters over ocean (Fig. 11) and for
488 high and mid-level clouds over land (Fig. 12). Over frozen surfaces (Fig. 13), the sounder clouds
489 show optically thin and high clouds, especially in CLIMCAPS V2; a large percentage of mid-level
490 clouds with medium to large ECF values are seen in AIRS V7, more consistent with the cloud
491 histograms from imager observations. However, MODIS and VIIRS cloud detection and retrievals
492 suffer a higher uncertainty over frozen surfaces (Chan and Comiso, 2013), and the small
493 atmospheric thermal contrast with frozen surfaces presents additional challenges for hyperspectral
494 IR sounder retrievals (Yue and Lambrigtsen 2020). Therefore, more accurate cloud measurements



495 from in-situ or active space-borne instruments are needed to further quantify the quality of these
496 imager and sounder cloud retrieval products in snow- and ice-covered regions.

497 Because of its long temporal coverage since 1999 when *Terra* MODIS began operating, high
498 quality, and the distinct physical characteristics of different cloud types, the MODIS cloud data
499 record, especially the CTP-COD joint histograms, have been widely used in different aspects of
500 climate studies. These include detailed analyses on the radiative effect of different cloud types
501 (Yue et al. 2016, Oreopoulos et al. 2016), evaluation of climate model simulations of clouds
502 (Pincus et al. 2012), quantification of the cloud feedback by different cloud types (Zhou et al. 2014,
503 Yue et al. 2019), and investigations of cloud impacts on hydrological cycle and the global
504 circulation (Su et al. 2017), especially in the tropics. Therefore, the differences of the cloud
505 frequency histograms from various imager retrieval products in the tropics are further analyzed
506 here. In Fig. 14, the MODIS continuity product (depicted in Fig. 10) is used as the common base
507 to evaluate the differences caused by algorithms and sensors: 1) between current NASA standard
508 MODIS retrievals and the MODIS continuity algorithms, and 2) between the MODIS and VIIRS
509 continuity cloud data records. The magnitude of joint frequency histogram differences is within
510 $\pm 5\%$ using the focus day observations. MYD06 shows more clouds with CTP < 180 hPa but fewer
511 low clouds with CTP > 800 hPa than the continuity product, consistent with findings in Platnick
512 et al. (2021). VIIRS continuity cloud retrievals produce higher frequencies of clouds with COD
513 between 9.4 and 60, but fewer high clouds with COD < 9.4. Whether and how these differences
514 will impact the long-term trend and short-term variability of clouds as seen by the imagers warrants
515 further study.

516 3.4.2 Cloud thermodynamic phase



517 Both MYD06 and continuity cloud products provide cloud thermodynamic phases (Table 1),
518 given by the optical property retrieval (Cloud_Phase_Optical_Properties, in both MYD06 and
519 continuity products) and the CLAVR-x processing system (Cloud_Phase_Cloud_Top_Properties,
520 continuity products only). The Cloud_Phase_Cloud_Top_Properties variable reports flags
521 determining pixels to be cloud free, water cloud, ice cloud, mixed phase cloud, or undetermined
522 phase. The Cloud_Phase_Optical_Properties flags indicate cloud mask not determined for pixel,
523 clear sky, liquid water cloud, ice cloud, or undetermined phase, the last of which includes mixed
524 phase clouds (Marchant et al. 2016). AIRS thermodynamic cloud phase, which is available in the
525 AIRS V6 and V7 Level 2 Support product, is based on a set of brightness temperature difference
526 and threshold tests using the channels in 960, 1231, 930, and 1227 cm^{-1} (Nasiri and Kahn 2008,
527 Kahn et al. 2014). These tests are applied to AIRS FOVs where $\text{ECF} > 0.01$, and classify the AIRS
528 FOV as containing liquid, ice, or unknown cloud phases. Detailed comparisons of AIRS cloud
529 phases with CALIPSO indicate good agreement with CALIPSO on ice phase detection, and
530 conservative liquid phase determination (Jin and Nasiri 2014, Peterson et al. 2020). These studies
531 also show that the unknown class of AIRS cloud phase corresponds to scenes containing both ice
532 and liquid particles, and low-level liquid clouds, especially in the trade-wind cumulus cloud regime.

533 Figs. 15-18 show the histograms of cloud thermodynamic phase (solid color bars for imagers
534 and magenta symbols for AIRS) for the same set of focus-day SNOs. Similar to joint histograms
535 in Fig. 10-13, each figure shows results over the four types of surfaces and regions: tropics, ocean,
536 land, and frozen surfaces. MODIS and VIIRS cloud mask histograms (hollow color bars) are also
537 shown in the figures, together with the frequency of clear sky detected by IR sounders ($\text{ECF} <$
538 0.01 , colored solid circles). Note that for MODIS and VIIRS, the mixed-phase or undetermined
539 phase category is shown with the y-axis on the right due to their much smaller frequency of



540 occurrence. For clear sky detection, the cloud-mask clear frequencies from all the imager products
541 are similar except over the frozen surfaces, where VIIRS cloud mask shows 10% higher frequency
542 than MODIS. For IR sounders, AIRS V7 produces significantly lower clear-sky frequency than
543 CLIMCAPS and imager cloud products over non-frozen surfaces. Over frozen surfaces, more
544 frequent clear conditions are reported by AIRS V7 than CLIMCAPS, although AIRS V7 is more
545 consistent with the clear frequency from MODIS and VIIRS data.

546 The frequencies of liquid or ice phase clouds are highly consistent between two cloud phase
547 variables in various imager cloud products, except for ice phase determination over frozen surfaces.
548 This is supported by the low uncertainty range of ice and liquid phase for these four conditions as
549 shown in Table 3. Here uncertainty is roughly characterized by the standard deviation of estimates
550 from different products and variables. The Cloud_Phase_Cloud_Top_Properties reports higher
551 percentage of liquid phase than Cloud_Phase_Optical_Properties. In particular, the VIIRS cloud
552 top cloud phase product always reports the highest frequency of liquid clouds. From both cloud
553 phase variables, MODIS reports more ice and fewer liquid clouds than VIIRS. When looking at
554 Cloud_Phase_Optical_Properties for MODIS, ice (liquid) cloud frequency is higher (lower) in
555 MYD06 than in the CLDPROP_MODIS products. The undetermined phase by the
556 Cloud_Phase_Optical_Properties includes both mixed and uncertain phases (Baum et al. 2012).
557 Except in tropics, MYD06 has the higher frequency of undetermined cases than the continuity
558 cloud products, and this is most prominent over the frozen surfaces with MYD06 reporting ~2.8%.

559 AIRS cloud phase retrievals report a higher frequency of ice clouds than imagers under all
560 conditions, especially in the tropics (Fig. 15) and over land (Fig. 17). However, a much lower
561 frequency of liquid clouds is retrieved by AIRS, which is consistent with a more conservative
562 liquid phase determination approach applied by AIRS cloud phase algorithm (Kahn et al. 2014).



563 The unknown phase of AIRS ranges from ~15% over the frozen surfaces to ~45% over ocean and
564 in the tropics, which corresponds with broken and thin low clouds and scenes with both ice and
565 liquid cloud particles (Jin and Nasiri 2014).

566

567 **4. Summary**

568 In this study, the pixel-scale collocation between the hyperspectral infrared (IR) sounders
569 (AIRS and CrIS) and high spatial resolution imagers (MODIS and VIIRS) is performed on the
570 pairs of Simultaneous Nadir Observations (SNOs) between *Aqua*-AIRS and *SNPP*-CrIS. Using
571 this approach, the cloud parameters retrieved by various algorithms for IR sounders and imagers
572 from different platforms are evaluated at the pixel level. Quantifying uncertainty in the cloud
573 observational data records is important for constraining the high uncertainty of clouds in weather
574 and climate research. This is also crucial in improving the retrieval of atmospheric, surface, and
575 radiation properties since satellite observations are highly subject to uncertainties and limitations
576 associated with cloud conditions in the instrument field of view (FOV) (e.g. Yue et al. 2013, Wong
577 et al. 2015, Tian et al, 2020). Moreover, narrowband imagers and hyperspectral sounders provide
578 important components of the long-term sustained observations of cloud properties in the Program
579 of Record (POR), as noted by the 2017 US National Academy Decadal Survey (ESAS 2017). The
580 analyses presented here will help to assess the capability of the POR, thus to identify potential
581 gaps existed in the POR for cloud properties.

582 Both the NASA standard and continuity retrieval algorithms for sounders and imagers are
583 investigated here in order to quantify the differences among the retrieval products, and to examine
584 the consistency and continuity of the data products from multiple sensors across different satellites.
585 This is essential to the goal of building a continuous record of satellite data using the *Terra*, *Aqua*,



586 *SNPP*, and *JPSS* series satellites, with sufficient quality to detect and quantify global
587 environmental change.

588 Multiple cloud parameters are analyzed (Table 1). Comparisons are made by investigating the
589 mean cloud parameters, and higher statistical moments of cloud property distributions measured
590 by MODIS and VIIRS over the corresponding AIRS and CrIS FOV. Cloud types indicated by the
591 joint histograms of cloud properties and cloud thermodynamic phases are included. Through these
592 comparisons, good agreement is found between the sounder and imager retrieved cloud products,
593 yet with distinct differences likely arising from algorithm and sensor differences. For IR sounders,
594 cloud top pressure (CTP) retrieved by AIRS Version 7 (V7) and CLIMCAPS (*-Aqua* and *-SNPP*)
595 Version 2 (V2) agree, as shown by correlation coefficients of 0.69 for all cases and 0.92 for cases
596 with effective cloud fraction (ECF) greater than 0.1, respectively. Compared to AIRS V7,
597 CLIMCAPS tends to produce a lower cloud top (CTP 12 hPa larger) for low clouds, but higher
598 cloud top (CTP 13 hPa smaller) for high clouds. However, CLIMCAPS V2 significantly
599 overestimates the frequency of clear and optically thin cloud (ECF < 0.1), relative to AIRS V7 and
600 imager products from both MODIS and VIIRS. This is due to the algorithmic differences between
601 CLIMCAPS V2 and AIRS V7 cloud retrieval algorithms. These differences include whether
602 iteration of cloud clearing is performed, the surface/atmospheric states used in the cloud retrieval,
603 the quality control procedures used, and different *a-priori* states used by AIRS V7 and CLIMCAPS.
604 How these differences affect the downstream atmospheric and surface retrievals in the two
605 algorithms, and the attribution of impacts from each factor, is beyond the scope of this study and
606 warrants further investigation.

607 High consistency is seen among different imager cloud products, especially in the mean and
608 standard deviation of cloud properties from the MODIS atmosphere cloud property retrieval



609 (MYD06) and the MODIS-VIIRS continuity cloud products (CLDPROP). The magnitude of the
610 correlation coefficients closely reflects the impact of algorithm differences and instrument spectral
611 and resolution differences, with highest correlations obtained between two MODIS products (same
612 sensor but different algorithms) and lowest between MYD06 and CLDPROP_VIIRS (different
613 sensors, different algorithms). The correlation coefficients are always higher for cloud optical
614 depth (COD) and particle effective radius (R_e) than for CTP. For mean cloud properties, they are
615 as large as 0.97 between MYD06 and CLDPROP_MODIS, and 0.89 for CTP. For standard
616 deviations within the sounder FOV, the correlations are smaller than those for mean cloud
617 properties, ranging from 0.77 to 0.96 for COD, 0.66 to 0.97 for R_e , but only 0.60 to 0.63 for CTP.
618 This is likely due to the fact that completely different CTP retrieval methods are used in the
619 MODIS operational and continuity cloud algorithms to accommodate the lack of near-IR and IR
620 water vapor and CO_2 absorption channels in VIIRS. Such algorithm and instrument impacts are
621 more apparent in the higher moment statistics of cloud properties such as skewness. The
622 correlations of COD and R_e skewness between MYD06 and CLDPROP_MODIS drop to 0.78 and
623 0.70, respectively. They are further reduced to below 0.4 when comparing MODIS and VIIRS
624 cloud products. For CTP skewness, the correlation coefficients are less than 0.3.

625 Two different cloud thermodynamic phase retrievals are available from imager observations,
626 which are obtained by the optical property retrieval (Cloud_Phase_Optical_Properties, in both
627 MYD06 and MODIS-VIIRS continuity products) and the CLAVR-x processing system
628 (Cloud_Phase_Cloud_Top_Properties, continuity products only). The frequencies of liquid or ice
629 phase clouds are very consistent between two cloud phase variables in different imager cloud
630 products, with uncertainty usually generally less than 4%. The largest uncertainty is reported for
631 ice phase determination over snow and ice covered surfaces. MODIS retrievals report more ice



632 and fewer liquid clouds than VIIRS, consistent with findings by Platnick et al. (2020). Comparing
633 the two different cloud phase retrievals, the Cloud_Phase_Cloud_Top_Properties reports higher
634 percentages of liquid phase than Cloud_Phase_Optical_Properties, and the
635 Cloud_Phase_Optical_Properties in MYD06 detects higher (lower) frequencies of ice (liquid)
636 clouds than that in the CLDPROP_MODIS products.

637 The general consistency of cloud observations among different sensors aboard *Aqua* and *SNPP*
638 from various algorithms is encouraging, especially for achieving a continuous multi-decadal
639 climate data record of clouds that can extend beyond the A-Train era and well into the 2030s with
640 the *JPSS* series. The quantification of algorithm differences has important implications for future
641 retrieval algorithm developments, and will further improve the capability and accuracy of such
642 climate data records.

643

644 **Data and Code Availability:**

645 MODIS (MYD06 10.5067/MODIS/MYD06_L2.061; MYD35
646 10.5067/MODIS/MYD35_L2.061; CLDPROP-MODIS
647 10.5067/VIIRS/CLDPROP_L2_MODIS_Aqua.011; CLDMSK-MODIS
648 10.5067/MODIS/CLDMSK_L2_MODIS_Aqua.001) and VIIRS data (CLDPROP-VIIRS
649 10.5067/VIIRS/CLDPROP_L2_VIIRS_SNPP.011; CLDMSK-VIIRS
650 10.5067/VIIRS/CLDMSK_L2_VIIRS_SNPP.001) were obtained through the Level-1
651 Atmosphere Archive and Distribution System (LAADS; <http://ladsweb.nascom.nasa.gov/>). AIRS
652 (AIRS V7 Level 2 Support Product [10.5067/APJ6EEN0PD0Z](https://doi.org/10.5067/APJ6EEN0PD0Z); CLIMCAPS-Aqua Version 2
653 Level 2 [10.5067/JZMYK5SMYM86](https://doi.org/10.5067/JZMYK5SMYM86)) and CrIS data (CLIMCAPS-SNPP Version 2 FSR
654 [10.5067/62SPJFQW5Q9B](https://doi.org/10.5067/62SPJFQW5Q9B); CLIMCAPS-SNPP Version 2 NSR [10.5067/8RUZ11F8U1UX](https://doi.org/10.5067/8RUZ11F8U1UX)) were



655 obtained from the NASA Goddard Earth Sciences Data Information and Services Center
656 (GESDISC) and could be accessed at <https://earthdata.nasa.gov/>. The collocation code is publicly
657 available from https://github.com/wanglikun1973/CriS_VIIRS_collocation. The data used to
658 generate the figures and tables in this study can be obtained by contacting the corresponding
659 author.

660

661 **Author Contribution:**

662 QY conceptualized the study, developed the methodology and datasets, carried out the formal
663 analyses, and contributed to the writing of the manuscript. EF, BK, NS, JB, and BL contributed
664 to the data curation, validation, investigation, and the writing of the manuscript. LW, IT, MM,
665 and KM contributed to the data curation and software.

666

667 **Competing Interests:**

668 The authors declare that they have no conflict of interest
669

670 **Acknowledgements:**

671 The research was carried out at the Jet Propulsion Laboratory, California Institute of
672 Technology, under a contract with the National Aeronautics and Space Administration
673 (80NM0018D0004). QY, EJF, BHK, and BL were supported by NASA's Making Earth Science
674 Data Records for Use in Research Environments (MEaSUREs) program. QY was supported by
675 the NASA CloudSat and CALIPSO Science Team Recompete NNH15ZDA001N-CCST grant.
676 QY, EJF, MS, and BHK acknowledge the support of the AIRS Project at JPL and the sounder
677 SIPS at JPL.



678 **References**

- 679
680 Baum, B. A., Menzel, W. P., Frey, R. A., Tobin, D. C., Holz, R. E., Ackerman, S. A., Heidinger,
681 A. K., and Yang, P.: MODIS Cloud-Top Property Refinements for Collection 6, *Journal of*
682 *Applied Meteorology and Climatology*, 51(6), 1145-1163, 2012.
- 683 Bony, S., and co-authors: *Clouds, circulation and climate sensitivity*. Nature Geoscience, 261-
684 268, doi:10.1038/ngeo2398, 2015.
- 685 Chahine, M. T.: Remote sounding of cloudy atmospheres. I. The single cloud layer, *J. Atmos.*
686 *Sci.*, 31, 233–243, 1974.
- 687 Chan, M. A., and Comiso, J. C.: Arctic Cloud Characteristics as Derived from MODIS,
688 CALIPSO, and CloudSat, *Journal of Climate*, 26(10), 3285-3306, 2013.
- 689 Eresmaa, R.: Imager-assisted cloud detection for assimilation of infrared atmospheric sounding
690 interferometer radiances. *Q. J. R. Meteorol. Soc.* 140, 2342–2352, 2014.
- 691 ESAS 2017: National Academies of Sciences, Engineering, and Medicine (2017). Thriving on
692 Our Changing Planet: A Decadal Strategy for Earth Observation from Space. Washington,
693 DC: *The National Academies Press*. <https://doi.org/10.17226/24938>.
- 694 Fetzer, E. J., Lambrigtsen, B. H., Eldering, A., Aumann, H. H., and Chahine, M. T.: Biases in
695 total precipitable water vapor climatologies from Atmospheric Infrared Sounder and
696 Advanced Microwave Scanning Radiometer, *J. Geophys. Res.*, 111, D09S16,
697 doi:10.1029/2005JD006598, 2006.
- 698 Fetzer, E. J., Yue, Q., Thrastarson, H. Th., and Ruzmaikin, A., ed., 2020: ALGORITHM
699 THEORETICAL BASIS DOCUMENT AIRS-Team Retrieval For Core Products and
700 Geophysical Parameters: Versions 6 and 7 Level2, available at:
701 https://docserver.gesdisc.eosdis.nasa.gov/public/project/AIRS/L2_ATBD.pdf



- 702 Fishbein, E., Lee, S-Y., and Fetzer, E. J., 2001: Atmospheric Infrared Sounder (AIRS) Level 2
703 Simulation System Description Document, available at:
704 http://asl.umbc.edu/pub/airs/jpldocs/sim/AIRS_L2_Simulation_Desc.pdf.
- 705 Frey, R. A., Ackerman, S. A., Holz, R. E., Steven, D., and Griffith, Z.: The Continuity MODIS-
706 VIIRS Cloud Mask, *Remote Sens.* 12, no. 20: 3334. <https://doi.org/10.3390/rs12203334>,
707 2020.
- 708 Gelaro, R., McCarty, W., Suárez, M. J., Todling, R., Molod, A., Takacs, L., Randles, C. A.,
709 Darmenov, A., Bosilovich, M. G., Reichle, R., Wargan, K., Coy, L., Cullather, R., Draper,
710 C., Akella, S., Buchard, V., Conaty, A., da Silva, A. M., Gu, W., Kim, G.-K., Koster, R.,
711 Lucchesi, R., Merkova, D., Nielsen, J. E., Partyka, G., Pawson, S., Putman, W., Rienecker,
712 M., Schubert, S. D., Sienkiewicz, M., and Zhao, B.: The modern-era retrospective analysis
713 for research and applications, Version 2 (MERRA-2), 30, 5419–5454,
714 <https://doi.org/10.1175/JCLI-D-16-0758.1>, 2017.
- 715 Gong, X., Li, Z., Li, J., Moeller, C. C., Cao, C., Wang, W., and Menzel, W. P.: Intercomparison
716 between VIIRS and CrIS by taking into account the CrIS subpixel cloudiness and viewing
717 geometry. *Journal of Geophysical Research: Atmospheres*, 123, 5335– 5345.
718 <https://doi.org/10.1029/2017JD027849>, 2018.
- 719 Heidinger, A. K., Evan, A. T., Foster, M. J., and Walther, A.: A naive Bayesian cloud detection
720 scheme derived from CALIPSO and applied with PATMOS-x, *J. Appl. Meteorol. Clim.*, 51,
721 1129–1144, 2012.
- 722 Heidinger, A. K., Foster, M. J., Walther, A., and Zhao, X.: The Pathfinder Atmospheres-
723 Extended AVHRR climate dataset, *B. Am. Meteorol. Soc.*, 95, 909-922,
724 <https://doi.org/10.1175/BAMS-D-12-00246.1>, 2014.



- 725 Holz, R. E., Ackerman, S. A., Nagle, F. W., Frey, R., Dutcher, S., Kuehn, R. E., Vaughan, M. A.
726 and Baum B.: Global Moderate Resolution Imaging Spectroradiometer (MODIS) cloud
727 detection and height evaluation using CALIOP, *J. Geophys. Res.*, 113, D00A19,
728 doi:10.1029/2008JD009837, 2008.
- 729 Hook, S.: Combined ASTER and MODIS Emissivity database over Land (CAMEL) Emissivity
730 Monthly Global 0.05Deg V002,
731 <https://doi.org/10.5067/MEASURES/LSTE/CAM5K30EM.002>, 2019
- 732 IPCC (2013). Climate Change 2013: The Physical Science Basis. Contribution of Working
733 Group I to the Fifth Assessment Report of the Intergovernmental Panel on Climate Change
734 [Stocker, T.F., D. Qin, G.-K. Plattner, M. Tignor, S.K. Allen, J. Boschung, A. Nauels, Y.
735 Xia, V. Bex and P.M. Midgley (eds.)]. Cambridge University Press, Cambridge, United
736 Kingdom and New York, NY, USA, 1535 pp, doi:10.1017/CBO9781107415324, 2013.
- 737 Irion, F. W., Kahn, B. H., Schreier, M. M., Fetzer, E. J., Fishbein, E., Fu, D., Kalmus, P., Wilson,
738 R. C., Wong, S., and Yue, Q.: Single-footprint retrievals of temperature, water vapor and
739 cloud properties from AIRS, *Atmos. Meas. Tech.*, 11, 971–995, [https://doi.org/10.5194/amt-](https://doi.org/10.5194/amt-11-971-2018)
740 [11-971-2018](https://doi.org/10.5194/amt-11-971-2018), 2018.
- 741 Jin, H. C., and Nasiri, S. L.: Evaluation of AIRS cloud-thermodynamic-phase determination with
742 CALIPSO. *J. Appl. Meteor. Climatol.*, 53, 1012–1027, [https://doi.org/10.1175/JAMC-D-13-](https://doi.org/10.1175/JAMC-D-13-0137.1)
743 [0137.1](https://doi.org/10.1175/JAMC-D-13-0137.1), 2014.
- 744 Kahn, B. H., Irion, F. W., Dang, V. T., Manning, E. M., Nasiri, S. L., Naud, C. M., Blaisdell, J.
745 M., Schreier, M. M., Yue, Q., Bowman, K. W., Fetzer, E. J., Hulley, G. C., Liou, K. N.,
746 Lubin, D., Ou, S. C., Susskind, J., Takano, Y., Tian, B., and Worden, J. R.: The Atmospheric



- 747 Infrared Sounder version 6 cloud products, *Atmos. Chem. Phys.*, 14, 399–426,
748 <https://doi.org/10.5194/acp-14-399-2014>, 2014.
- 749 Kahn, B. H., Schreier, M. M., Yue, Q., Fetzer, E. J., Irion, F. W., Platnick, S., Wang, C., Nasiri,
750 S. L., and L'Ecuyer, T. S.: Pixel-scale assessment and uncertainty analysis of AIRS and
751 MODIS ice cloud optical thickness and effective radius, *J. Geophys. Res. Atmos.*, 120,
752 11,669– 11,689, doi:[10.1002/2015JD023950](https://doi.org/10.1002/2015JD023950), 2015.
- 753 Kahn, B. H., Matheou, G., Yue, Q., Fauchez, T., Fetzer, E. J., Lebsock, M., Martins, J., Schreier,
754 M. M., Suzuki, K., and Teixeira, J.: An A-train and MERRA view of cloud, thermodynamic,
755 and dynamic variability within the subtropical marine boundary layer, *Atmos. Chem. Phys.*,
756 17, 9451–9468, <https://doi.org/10.5194/acp-17-9451-2017>, 2017.
- 757 Kawai, H. and Teixeira, J.: Probability density functions of liquid water path and cloud amount
758 of marine boundary layer clouds: Geographical and seasonal variations and controlling
759 meteorological factors, *J. Clim.*, 23, 2079–2092, 2010.
- 760 Li, J., Menzel, W. P., Sun, F., Schmit, T. J., and Gurka, J.: AIRS Subpixel Cloud
761 Characterization Using MODIS Cloud Products, *Journal of Applied Meteorology*, 43(8),
762 1083-1094, 2004.
- 763 Manning, E. M., and Aumann H. H: Tropical simultaneous nadir observations for IR sounder
764 evaluation and comparison, *Proc. SPIE, Earth Observing Systems*, 96070L (8 September
765 2015); <https://doi.org/10.1117/12.2187151>, 2015.
- 766 Marchant, B., Platnick, S., Meyer, K., Arnold, G. T., and Riedi, J: MODIS Collection 6
767 shortwave-derived cloud phase classification algorithm and comparisons with CALIOP.
768 *Atmospheric Measurement Techniques*, 9(4), 1587–1599. [http://doi.org/10.5194/amt-9-1587-](http://doi.org/10.5194/amt-9-1587-2016)
769 [2016](http://doi.org/10.5194/amt-9-1587-2016), 2016.



- 770 Masuda, K., Takashima, T. and Takayama, Y.: Emissivity of pure and sea waters for the model
771 sea surface in the infrared window regions, *Remote Sensing Environ.* 24, 313–329.
772 [https://doi.org/10.1016/0034-4257\(88\)90032-6](https://doi.org/10.1016/0034-4257(88)90032-6), 1988.
- 773 McCoy, D. T., Eastman, R., Hartmann, D. L., and Wood, R: The change in low cloud cover in a
774 warmed climate inferred from AIRS, MODIS, and ERA-interim, *Journal of Climate*, 30(10),
775 3609-3620. <https://dx.doi.org/10.1175/JCLI-D-15-0734.1>, 2017.
- 776 Milstein, A.B., and Blackwell, W. J.: Neural network temperature and moisture retrieval
777 algorithm validation for AIRS/AMSU and CrIS/ATMS, *J. Geophys. Res. Atmos.*, 121, 1414-
778 1430, doi: 10.1002/2015JD024008, 2016.
- 779 Monarrez, R., ed., 2020: NASA-SNPP and NOAA-20 (JPSS-1) CLIMCAPS CrIS and ATMS
780 Level-2 Products User Guide: File Format and Definition, available at:
781 [https://docserver.gesdisc.eosdis.nasa.gov/public/project/Sounder/CLIMCAPS.V2.README.](https://docserver.gesdisc.eosdis.nasa.gov/public/project/Sounder/CLIMCAPS.V2.README.pdf)
782 [pdf](https://docserver.gesdisc.eosdis.nasa.gov/public/project/Sounder/CLIMCAPS.V2.README.pdf).
- 783 Nagle, F. W. and Holz, R. E.: Computationally Efficient Methods of Collocating Satellite,
784 Aircraft, and Ground Observations, *J. Atmos. Oceanic Technol.* (2009) 26 (8):1585–1595,
785 2009.
- 786 Nasiri, S. L., and Kahn, B. H.: Limitations of bispectral infrared cloud phase determination and
787 potential for improvement. *J. Appl. Meteor. Climatol.*, 47, 2895–2910,
788 <https://doi.org/10.1175/2008JAMC1879.1>, 2008.
- 789 Nasiri, S. L., Dang, V. T., Kahn, B. H., Fetzer, E. J., Manning, E. M., Schreier, M. M., and Frey,
790 R. A.: Comparing MODIS and AIRS Infrared-Based Cloud Retrievals, *Journal of Applied*
791 *Meteorology and Climatology*, 50(5), 1057-1072, 2011.



- 792 Oreopoulos, L., Cho, N., Lee, D., and Kato, S.: Radiative effects of global MODIS cloud
793 regimes, *J. Geophys. Res. Atmos.*, 121, 2299–2317, doi:[10.1002/2015JD024502](https://doi.org/10.1002/2015JD024502), 2016.
- 794 Oudrari, H., McIntire, J., Xiong, X., Butler, J., Lee, S., Lei, N., Schwarting, T., Sun, J.:
795 Prelaunch radiometric characterization and calibration of the SNPP VIIRS sensor. *IEEE*
796 *Trans. Geosci. Remote Sens.* **2015**, 53, 2195–2210, 2015.
- 797 Peterson, C. A., Yue, Q., Kahn, B. H., Fetzer, E., and Huang, X.: Evaluation of AIRS Cloud
798 Phase Classification over the Arctic Ocean against Combined CloudSat–CALIPSO
799 Observations, *Journal of Applied Meteorology and Climatology*, 59(8), 1277–1294, 2020.
- 800 Pincus, R., Platnick, S., Ackerman, S. A., Hemler, R. S., and Patrick Hofmann, R. J.:
801 Reconciling Simulated and Observed Views of Clouds: MODIS, ISCCP, and the Limits of
802 Instrument Simulators, *Journal of Climate*, 25(13), 4699–4720, 2012.
- 803 Platnick, S., Meyer, K. G., Yang, P., Ridgway, W. L., Riedi, J. C., King, M. D., Wind, G.,
804 Amarasinghe, N., Marchant, B., Arnold, G. T., et al.: The MODIS Cloud Optical and
805 Microphysical Products: Collection 6 Updates and Examples from Terra and *Aqua*. *IEEE*
806 *Trans. Geosci. Remote Sens.* **2017**, 55, 502–525, 2017.
- 807 Platnick, S., Meyer, K., Amarasinghe, N., Wind, G., Hubanks, P. A. and Holz, R. E.: Sensitivity
808 of Multispectral Imager Liquid Water Cloud Microphysical Retrievals to the Index of
809 Refraction, *Remote Sensing* 12, no. 24: 4165. <https://doi.org/10.3390/rs12244165>, 2020.
- 810 Platnick, S., Meyer, K., Wind, G., Holz, R. E., Amarasinghe, N., Hubanks, P. A., Marchant, B.,
811 Dutcher, S., and Veglio, P.: The NASA MODIS-VIIRS Continuity Cloud Optical Properties
812 Products. *Remote Sens.* 13, no. 1: 2. <https://doi.org/10.3390/rs13010002>, 2021.



- 813 Rossow, W. B., and Schiffer, R. A.: Advances in understanding clouds from ISCCP. *Bull. Amer.*
814 *Meteor. Soc.*, 80, 2261–2287,
815 [https://doi.org/10.1175/15200477\(1999\)080.2261:AIUCFL.2.0.CO;2](https://doi.org/10.1175/15200477(1999)080.2261:AIUCFL.2.0.CO;2), 1999.
- 816 Schreier, M. M.; Kahn, B. H.; Eldering, A.; Elliott, D. A.; Fishbein, E.; Irion, F. W.; Pagano, T.
817 S.: Radiance comparisons of MODIS and AIRS using spatial response information. *J. Atmos.*
818 *Oceanic Technol.* 2010, 27, 1331–1342, 2010.
- 819 Seemann, S. W., Borbas, E. E., Knuteson, R. O., Stephenson, G. R., and Huang, H.-L.:
820 Development of a Global Infrared Land Surface Emissivity Database for Application to Clear
821 Sky Sounding Retrievals from Multi-spectral Satellite Radiance Measurements. *J. Appl.*
822 *Meteor. Climatol.*, Vol. 47, 108-123, 2008.
- 823 Smith, N. and Barnet, C.D.: Uncertainty Characterization and Propagation in the Community
824 Long-Term Infrared Microwave Combined Atmospheric Product System (CLIMCAPS).
825 *Remote Sens.* **2019**, *11*, 1227, 2019.
- 826 Smith, N. and Barnet, C. D.: CLIMCAPS observing capability for temperature, moisture, and
827 trace gases from AIRS/AMSU and CrIS/ATMS, 13, 4437–4459, [https://doi.org/10.5194/amt-](https://doi.org/10.5194/amt-13-4437-2020)
828 [13-4437-2020](https://doi.org/10.5194/amt-13-4437-2020), 2020.
- 829 Smith, N., Esmaili, R., and Barnet, C. D. 2021: Community Long-Term Infrared Microwave
830 Combined Atmospheric Product System (CLIMCAPS) Science Application Guides,
831 available at:
832 https://docserver.gesdisc.eosdis.nasa.gov/public/project/Sounder/CLIMCAPS_V2_L2_scienc
833 [e_guides.pdf](https://docserver.gesdisc.eosdis.nasa.gov/public/project/Sounder/CLIMCAPS_V2_L2_scienc).



- 834 Su, H., and Coauthors: Tightening of Hadley ascent and tropical high cloud region key to
835 precipitation change in a warmer climate. *Nat. Commun.*, 8, 15771,
836 <https://doi.org/10.1038/ncomms15771>, 2017.
- 837 Susskind, J., Barnet, C. D., and Blaisdell, J. M.: Retrieval of atmospheric and surface parameters
838 from AIRS/AMSU/HSB data in the presence of clouds, *IEEE Trans. Geosci. Remote Sens.*,
839 41, 390–409, 2003.
- 840 Susskind, J., Barnet, C., Blaisdell, J., Iredell, L., Keita, F., Kouvaris, L. Molnar, G., and Chahine,
841 M.: Accuracy of geophysical parameters derived from Atmospheric Infrared
842 Sounder/Advanced Microwave Sounding Unit as a function of fractional cloud cover, *J.*
843 *Geophys. Res.*, 111, D09S17, doi:[10.1029/2005JD006272](https://doi.org/10.1029/2005JD006272), 2006.
- 844 Susskind, J., Blaisdell, J. M., and Iredell, L: Improved methodology for surface and atmospheric
845 soundings, error estimates, and quality control procedures: the atmospheric infrared sounder
846 science team version-6 retrieval algorithm, *Journal of Applied Remote Sensing* 8(1), 084994
847 (31 March 2014). <https://doi.org/10.1117/1.JRS.8.084994>, 2014.
- 848 Tian, B., and Hearty, T.: Estimating and removing the sampling biases of the AIRS Obs4MIPs
849 V2 data. *Earth and Space Science*, 7, e2020EA001438.
850 <https://doi.org/10.1029/2020EA001438>, 2020.
- 851 Thrastarson, H. Th., Fetzer, E. F., Ray, S., Hearty, T., and Smith, N., 2021: Overview of the
852 AIRS Mission: Instruments, Processing Algorithms, Products, and Documentation, 2nd
853 Edition. Available from:
854 [https://docserver.gesdisc.eosdis.nasa.gov/public/project/AIRS/Overview_of_the_AIRS_Miss](https://docserver.gesdisc.eosdis.nasa.gov/public/project/AIRS/Overview_of_the_AIRS_Mission.pdf)
855 [ion.pdf](https://docserver.gesdisc.eosdis.nasa.gov/public/project/AIRS/Overview_of_the_AIRS_Mission.pdf)



- 856 Thrastarson, H. Th., ed., 2021: AIRS/AMSU/HSB Version 7 Level 2 Product User Guide.
857 Available at:
858 [https://docserver.gesdisc.eosdis.nasa.gov/public/project/AIRS/V7_L2_Product_User_Guide.](https://docserver.gesdisc.eosdis.nasa.gov/public/project/AIRS/V7_L2_Product_User_Guide.pdf)
859 [pdf](https://docserver.gesdisc.eosdis.nasa.gov/public/project/AIRS/V7_L2_Product_User_Guide.pdf).
- 860 Tobin, D. C., Revercomb, H. E., Moeller, C. C., Pagano, T. S: Use of atmospheric infrared
861 sounder high-spectral resolution spectra to assess the calibration of moderate resolution
862 imaging spectroradiometer on EOS *Aqua*. *J. Geophys. Res. Atmos.* 2006, 111, 2006.
- 863 Wang, L., Tremblay, D. A., Han, Y., Esplin, M., Hagan, D. E., Predina, J., Suwinski, L., Jin, X.,
864 Chen, Y.: Geolocation assessment for CrIS sensor data records. *J. Geophys. Res. Atmos.*
865 2013, 118, 690–704, 2013.
- 866 Wang, L., Tremblay, D., Zhang, B., Han, Y.: Fast and Accurate Collocation of the Visible
867 Infrared Imaging Radiometer Suite Measurements with Cross-Track Infrared Sounder,
868 *Remote Sens.* 8, no. 1: 76. <https://doi.org/10.3390/rs8010076>, 2016.
- 869 Wang et al., ed., 2021: Test Report of Performance of CLIMCAPS-SNPP and CLIMCAPS-
870 JPSS1 Retrievals, available at:
871 [https://docserver.gesdisc.eosdis.nasa.gov/public/project/Sounder/CLIMCAPS.V2.Test.Repor](https://docserver.gesdisc.eosdis.nasa.gov/public/project/Sounder/CLIMCAPS.V2.Test.Report.pdf)
872 [t.pdf](https://docserver.gesdisc.eosdis.nasa.gov/public/project/Sounder/CLIMCAPS.V2.Test.Report.pdf).
- 873 Wong, S., Fetzer, E. J., Schreier, M., Manipon, G., Fishbein, E. F., Kahn, B. H., Yue, Q., and
874 Irion, F. W.: Cloud-induced uncertainties in AIRS and ECMWF temperature and specific
875 humidity, *J. Geophys. Res.*, 120, doi:10.1002/2014JD022440, 2015.
- 876 Wu, X. and Smith, W. L.: Emissivity of rough sea surface for 8–13 μm : modeling and
877 verification, *Appl. Opt.* **36**, 2609-2619. <https://doi.org/10.1364/AO.36.002609>, 1997.



- 878 Yao, Z., Li, J. and Zhao, Z.: Synergistic use of AIRS and MODIS for dust top height retrieval
879 over land. *Adv. Atmos. Sci.* **32**, 470–476, 2015. <https://doi.org/10.1007/s00376-014-4046-y>.
- 880 Yue, Q., Kahn, B. H., Xiao, H., Schreier, M. M., Fetzer, E. J., Teixeira, J., and Suselj, K.:
881 Transitions of cloud-topped marine boundary layers characterized by AIRS, MODIS, and a
882 large eddy simulation model. *Journal of Geophysical Research-Atmospheres*, 118(15), 8598-
883 8611, 2013.
- 884 Yue, Q., Kahn, B. H., Fetzer, E. J., and Teixeira, J.: Relationship between marine boundary
885 layer clouds and lower tropospheric stability observed by AIRS, CloudSat, and CALIOP.
886 *Journal of Geophysical Research-Atmospheres*, 116, 2011.
- 887 Yue, Q., Fetzer, E. J., Kahn, B. H., Schreier, M., Wong, S., Chen, X., and Huang, X.:
888 Observation-based Longwave Cloud Radiative Kernels Derived from the A-Train, *J.*
889 *Climate*, 29(6), 2023–2040, doi: <http://dx.doi.org/10.1175/JCLI-D-15-0257.1>, 2016.
- 890 Yue, Q., Kahn, B. H., Fetzer, E. J., Wong, S., Frey, R., and Meyer, K. G.: On the response of
891 MODIS cloud coverage to global mean surface air temperature. *Journal of Geophysical*
892 *Research-Atmospheres*, 122(2), 966-979, 2017.
- 893 Yue, Q., Fetzer, E. J., Kahn, B. H., Wong, S., Huang, X., and Schreier, M.: Temporal and Spatial
894 Characteristics of Short-term Cloud Feedback on Global and Local Interannual Climate
895 Fluctuations from A-Train Observations, *J. Climate*, DOI: [https://doi.org/10.1175/JCLI-D-](https://doi.org/10.1175/JCLI-D-18-0335.1)
896 [18-0335.1](https://doi.org/10.1175/JCLI-D-18-0335.1), 2019.
- 897 Yue, Q., and Lambriqtsen, B. ed., 2017: AIRS V6 Test Report Supplement: Performance of
898 AIRS+AMSU vs. AIRS-only Retrievals, available at:
899 https://docserver.gesdisc.eosdis.nasa.gov/repository/Mission/AIRS/3.3_ScienceDataProduct



900 [Documentation/3.3.5 ProductQuality/V6 Test Report Supplement Performance of AIRS](#)
901 [+AMSU vs AIRS-Only Retrievals.pdf](#).

902 Yue, Q., and Lambriqtsen, B. ed., 2020: AIRS V7 L2 Performance Test and Validation Report,
903 available at:

904 https://docserver.gesdisc.eosdis.nasa.gov/public/project/AIRS/V7_L2_Performance_Test_and_Validation_report.pdf.

906 Yue, Q. et al., ed., 2021: Version 2 CLIMCAPS-*Aqua* Retrieval Product Performance Test
907 Report, available at:

908 <https://docserver.gesdisc.eosdis.nasa.gov/public/project/Sounder/CLIMCAPS.V2.Test.Report.Aqua.pdf>.

910 Zelinka, M. D., Klein, S. A., and Hartmann D. L.: Computing and Partitioning Cloud Feedbacks
911 Using Cloud Property Histograms. Part I: Cloud Radiative Kernels. *J. Climate*, 25, 3715–3735,
912 2012.

913 Zhu, P., and Zuidema, P.: On the use of PDF schemes to parameterize sub-grid clouds, *Geophys.*
914 *Res. Lett.*, 36, L05807, doi:[10.1029/2008GL036817](https://doi.org/10.1029/2008GL036817), 2009.

915



916 Table 1: The satellite cloud parameters examined in this study, and the retrieval algorithms
 917 and products from which these parameters are obtained.

Satellite	Sensor	Retrieval Algorithm / Product	Cloud Parameters
<i>Aqua</i>	AIRS	AIRS Version 7 Level 2 Standard and Support Product	<ul style="list-style-type: none"> • Effective Cloud Fraction (ECF) • Cloud Top Pressure (CTP) • Cloud Thermodynamic Phase
		Version 2 CLIMCAPS- <i>Aqua</i> Level 2 Infrared and Microwave Combined Retrieval	<ul style="list-style-type: none"> • Effective Cloud Fraction (ECF) • Cloud Top Pressure (CTP)
	MODIS	Collection 6.1 <i>Aqua</i> MODIS Atmosphere Level 2 Cloud Product (MYD35, MYD06)	<ul style="list-style-type: none"> • Cloud Mask • Cloud Top Pressure (CTP) • Cloud Optical Depth (COD) • Cloud Effective Radius (Re) • Cloud Phase Optical Properties
		Version 1.1 NASA MODIS Continuity Cloud Mask and Cloud Property Products (CLDMSK/CLDPROP_MODIS)	<ul style="list-style-type: none"> • Cloud Mask • Cloud Top Pressure (CTP) • Cloud Optical Depth (COD) • Cloud Effective Radius (Re) • Cloud Phase Optical Properties • Cloud Phase Cloud Top Properties
<i>SNPP</i>	CrIS	Version 2 CLIMCAPS- <i>SNPP</i> FSR Level 2 Retrieval	<ul style="list-style-type: none"> • Effective Cloud Fraction (ECF) • Cloud Top Pressure (CTP)
		Version 2 CLIMCAPS- <i>SNPP</i> NSR Level 2 Retrieval	<ul style="list-style-type: none"> • Effective Cloud Fraction (ECF) • Cloud Top Pressure (CTP)
	VIIRS	Version 1.1 NASA VIIRS Continuity Cloud Mask and Cloud Property Products (CLDMSK/CLDPROP_VIIRS)	<ul style="list-style-type: none"> • Cloud Mask • Cloud Top Pressure (CTP) • Cloud Optical Depth (COD) • Cloud Effective Radius (Re) • Cloud Phase Optical Properties • Cloud Phase Cloud Top Properties

918
 919
 920



921

922

923

924

925 Table 2 Number of SNOs between *Aqua*-AIRS and *SNPP*-CrIS on the seven focus days used

926 in this study.

Focus Day	Jan. 01, 2016	Jan. 03, 2016	Jan 04, 2016	Jan 09, 2016	Jan 11, 2016	Jan 14, 2016	Jan 17, 2016
# of SNOs	10,000	10,000	1372	10,000	10,000	10,000	8,903

927

928

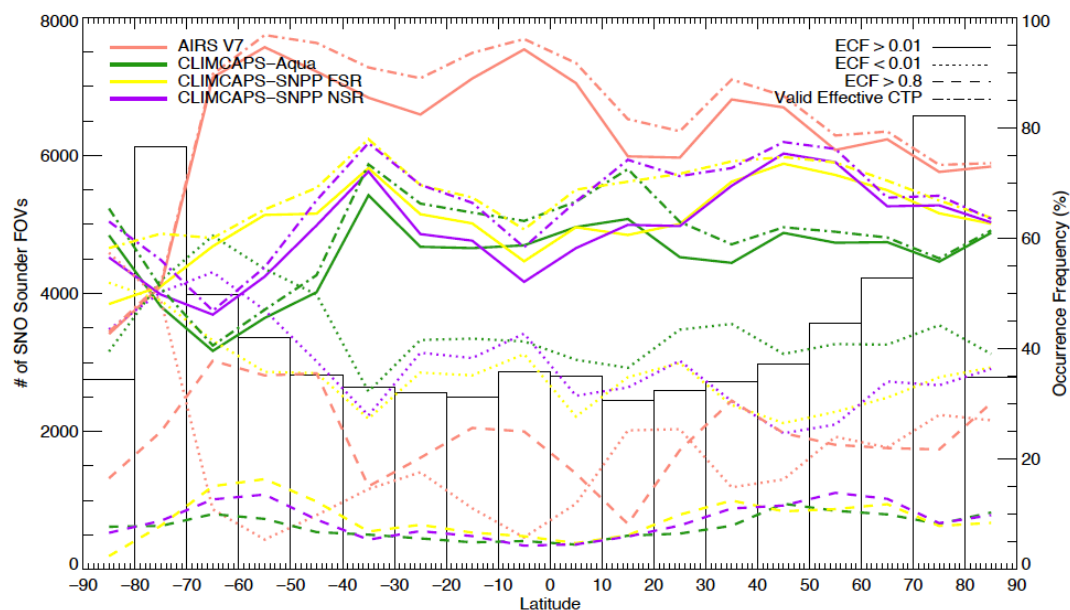


929 Table 3. The mean value and uncertainty range of the occurrence frequencies of ice and liquid
 930 phase clouds based on the cloud thermodynamic phase variables from the three imager cloud
 931 retrievals: MYD06, CLDRPOP_MODIS, and CLDPROP_VIIRS. Results over the five types of
 932 surfaces and regions are shown respectively for tropics, ocean, land, frozen surfaces, and global.
 933 For each condition, five estimates of cloud phase frequencies are available based on two types of
 934 imager-derived cloud thermodynamic phase: Cloud_Phase_Optical_Properties determined by the
 935 optical property retrieval (provided in both MYD06 and the two continuity products), and
 936 Cloud_Phase_Cloud_Top_Properties obtained through the CLAVR-x processing system applied
 937 in the continuity cloud algorithm (provided in the CLDPROP-MODIS and -VIIRS cloud
 938 products). The uncertainty range is characterized by the standard deviation of the five estimates
 939 obtained in each region.

940

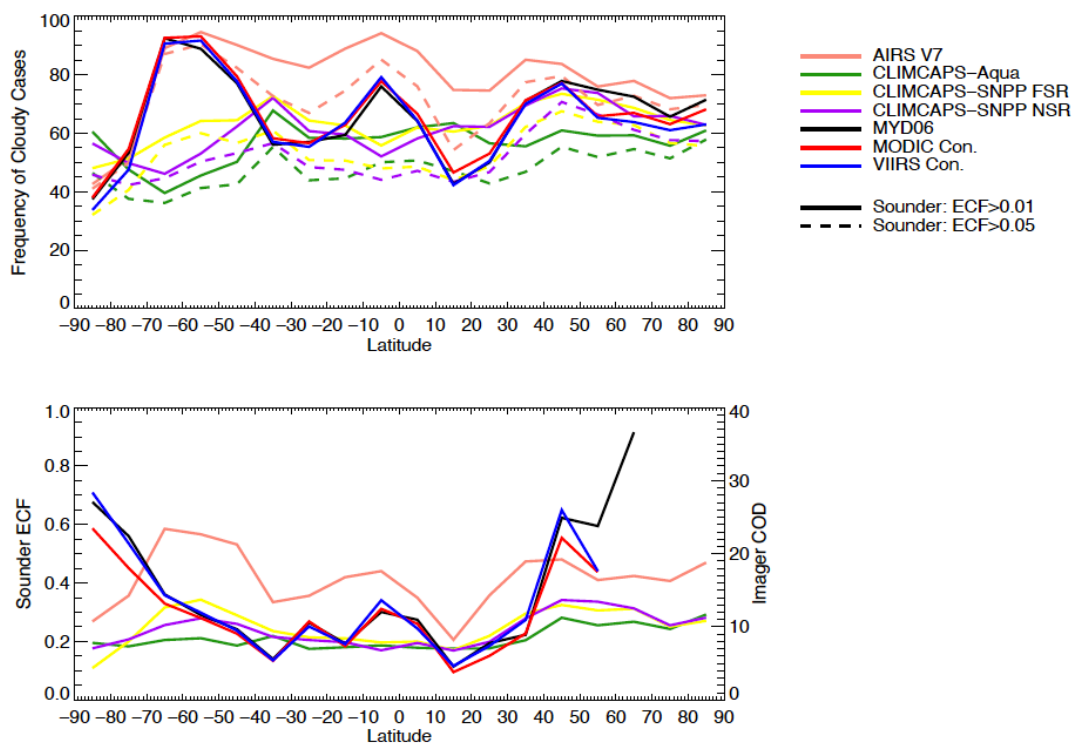
Frequency (%)	Tropics (30°N~30°S)	60°N~60°S Ocean	60°N~60°S Land	Frozen Surfaces	Global, All Cases
Liquid Phase	37.64±3.21	53.94±3.50	35.16±2.81	14.03±1.10	44.27±2.79
Ice Phase	26.36±1.96	21.32±2.59	23.37±1.03	14.28±4.38	20.43±3.02

941

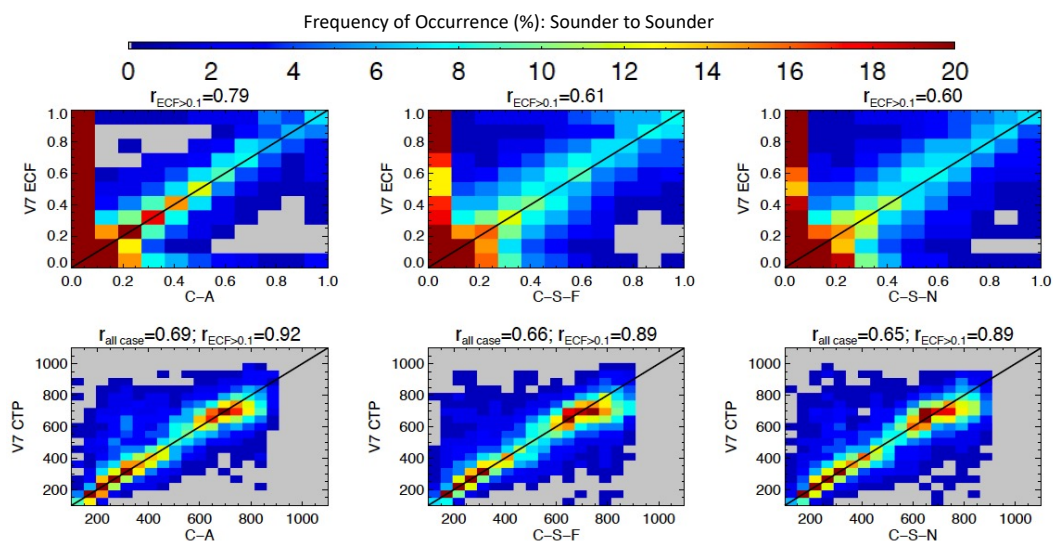


942
 943 Figure 1. The latitudinal distribution of the SNO pairs for *Aqua*-AIRS and *SNPP*-CrIS (black
 944 bars) and the occurrence frequencies of various sounder retrieved cloud parameters (right y-
 945 axis, %) for four composites that satisfy the following four conditions, respectively: ECF >
 946 0.01 (solid lines, general cloudy condition), ECF ≤ 0.01 (dotted lines, clear or very thin clouds),
 947 ECF > 0.8 (dash lines, overcast or very thick clouds), and cases with successful CTP retrievals
 948 (dash dotted lines, QC for CTP is 0 or 1). Data from the seven focus days are used (see Table 2)
 949 and binned by latitude of the sounder FOVs in 10° latitude bins. Four different sounder retrieval
 950 products are shown by colored lines: AIRS Version 7 (AIRS V7, pink), CLIMCAPS-*Aqua*
 951 (green), CLIMCAPS-*SNPP* FSR (yellow), and CLIMCAPS-*SNPP* NSR (purple). Occurrence
 952 frequency is calculated as the percentage of AIRS or CrIS FOVs with successful cloud retrievals
 953 (quality control indicator = 0 or 1) satisfying the aforementioned four conditions to the total
 954 number of FOVs in each latitudinal bin.

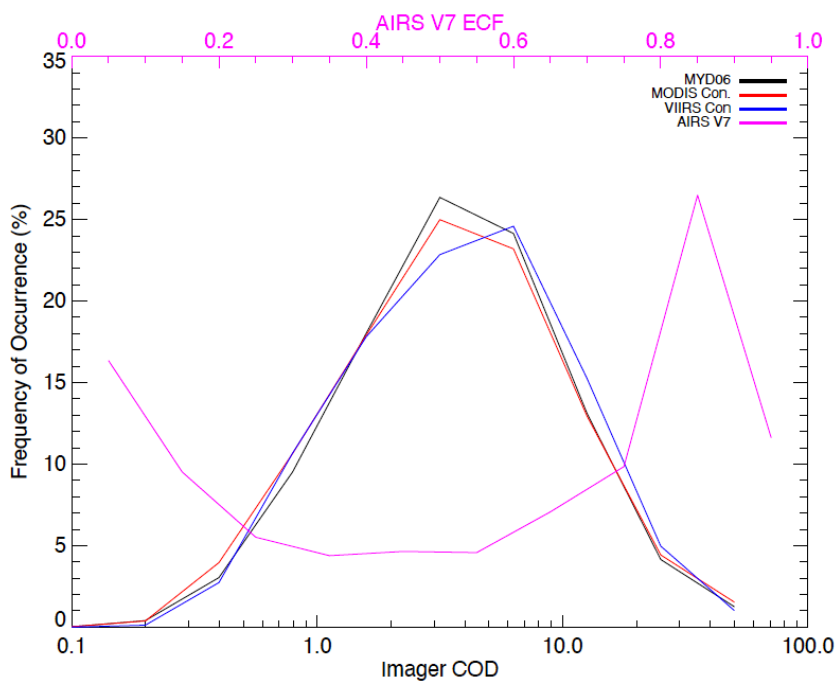
955
 956



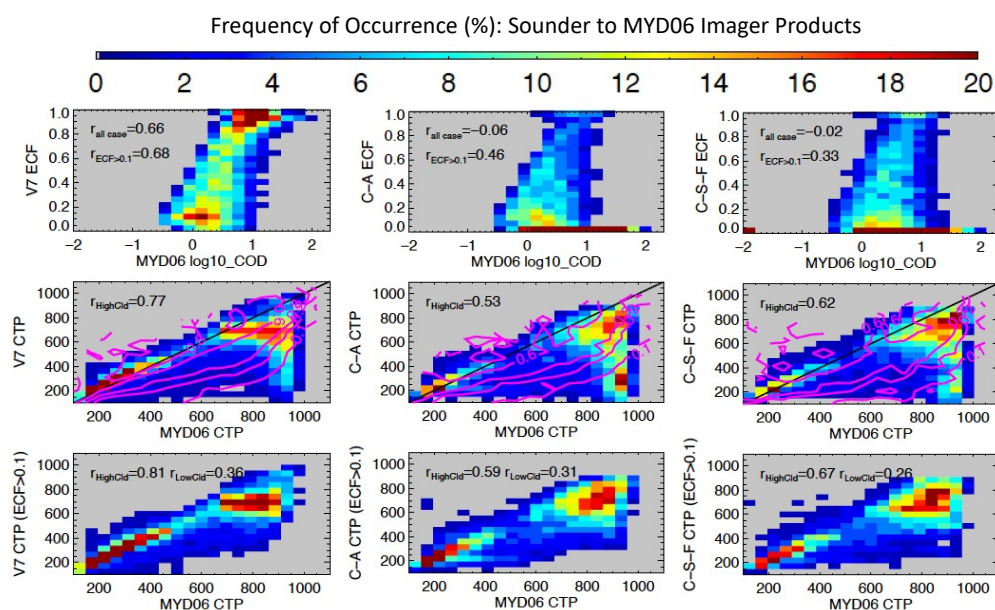
957
958 Figure 2. a) Zonal mean frequency of cloudy cases as observed by hyperspectral sounders and
959 imagers. For MODIS and VIIRS, frequency of Cloudy, Uncertain cases as reported by cloud
960 mask is shown for MYD06 (black), MODIS continuity (red), and VIIRS continuity (blue) cloud
961 products. For AIRS and CrIS, solid and dash lines show frequencies of sounder FOVs with
962 ECF > 0.01 and ECF > 0.05, respectively. Results for AIRS Version 7 (AIRS V7, pink),
963 CLIMCAPS-Aqua (green), CLIMCAPS-SNPP FSR (yellow), and CLIMCAPS-SNPP NSR
964 (purple) are shown for sounder cloud products. b) Zonal mean values of sounder ECFs (left y
965 axis) and imager COD (right y axis) from these retrieval algorithms.
966



967
 968 Figure 3. Comparisons of ECF (top row) and effective CTP (bottom row) derived from different
 969 sounder retrieval algorithms. Linear correlation coefficients are calculated for cloud properties
 970 obtained from retrieval products indicated on the axes and are given on top of the each plot.
 971 From left to right, results comparing AIRS Version 7 with CLIMCAPS-*Aqua* (C-A),
 972 CLIMCAPS-*SNPP* FSR (C-S-F), and CLIMCAPS-*SNPP* NSR (C-S-N) are shown using joint
 973 distributions of frequency of occurrence (%). The data points located in regions poleward of 60°
 974 are excluded. Cases are included only when both retrievals in comparison (x- and y-axes of the
 975 plot) report valid retrievals.
 976
 977

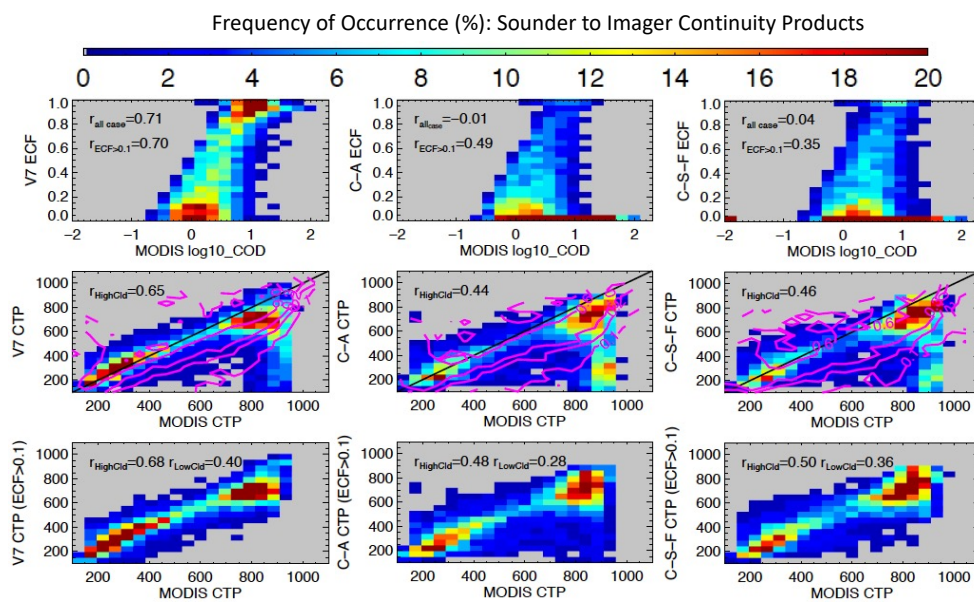


978
979 Figure 4. Frequency histograms showing the density distributions of imager cloud optical depth
980 (COD, bottom x-axis) and AIRS V7 ECF (magenta, upper x-axis) for cases where V2
981 CLIMCAPS-*Aqua* retrieves an ECF value less than 0.1. Different imager cloud products are
982 included: MYD06 (black), *Aqua*-MODIS continuity cloud products (MODIS Con., red), and
983 *SNPP*-VIIRS continuity cloud products (VIIRS Con., blue).
984



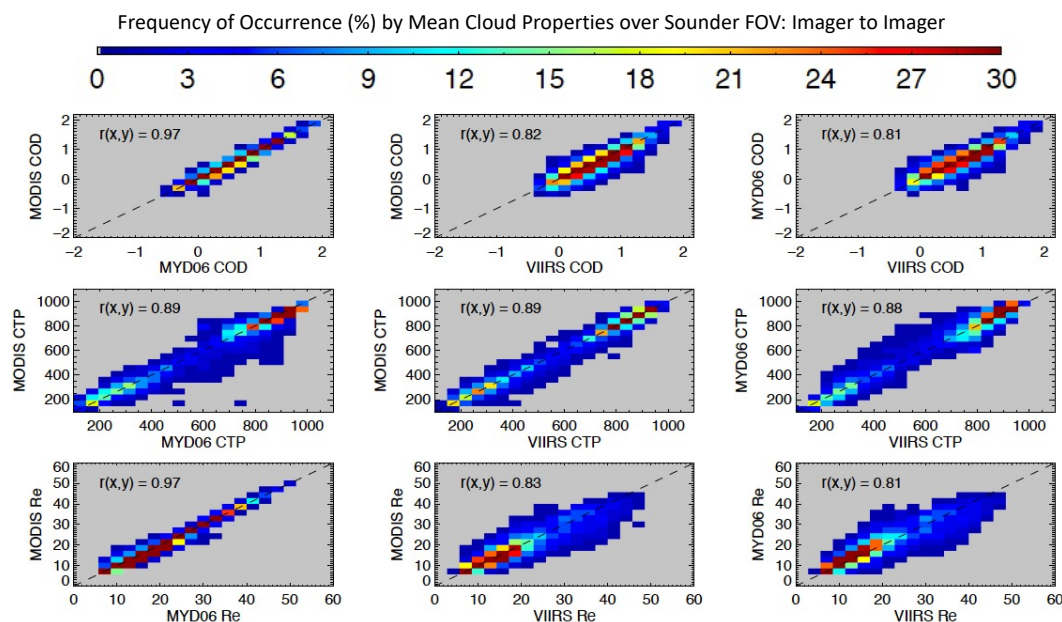
985
 986 Figure 5. Comparisons of sounder and imager derived cloud properties shown by joint
 987 distribution of case frequency of occurrence. Top row shows evaluation of sounder-derived ECF
 988 by cloud optical depth (COD, in log10 scale) from the MYD06 products. The middle row
 989 compares the sounder effective CTP with CTP from MYD06 overlaid by the magenta contours
 990 showing the mean ECF from the corresponding sounder retrievals. The bottom row is similar to
 991 the middle row except that the cases with sounder ECF < 0.1 are removed from the comparison.
 992 Different sounder retrieval algorithms are included. From left to right, data from AIRS Version
 993 7, CLIMCAPS-Aqua (C-A), and CLIMCAPS-SNPP FSR (C-S-F) are used. The data points
 994 located in regions poleward of 60° are excluded. Cases are included only when both retrievals in
 995 comparison (x- and y-axes of the plot) report valid retrievals. The cloud properties from MODIS
 996 pixels collocated within the same sounder FOV are averaged before comparing with the IR
 997 sounder data. Linear correlation coefficients between the variables on x- and y-axes for different
 998 conditions are given in each plot.

999
 1000



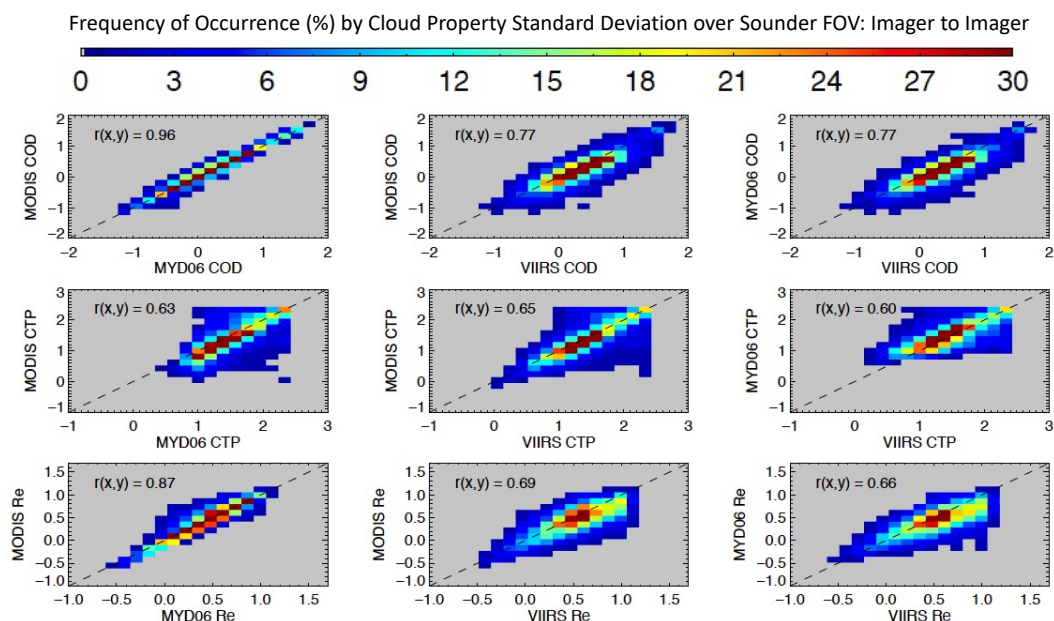
1001
 1002
 1003
 1004
 1005

Figure 6. Similar to Fig. 5, except using the MODIS continuity cloud product (CLDPROP_MODIS).



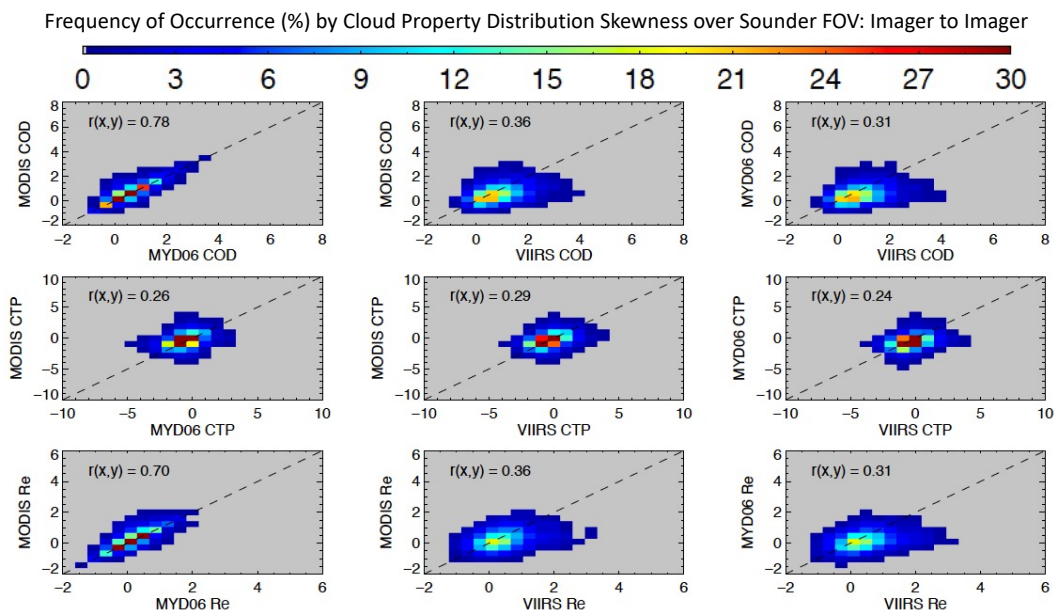
1006
1007
1008
1009
1010
1011
1012
1013
1014
1015

Figure 7. Comparison of cloud optical depth (COD, in log₁₀ scale), cloud top pressure (CTP, hPa), and effective particle size (Re, μm) retrieved by MODIS and VIIRS cloud algorithms. The mean imager cloud properties over corresponding sounder FOVs are compared over the SNOs. From left to right show the results of following comparisons: *Aqua* MODIS continuity cloud products (CLDPROP_MODIS) with MYD06, CLDPROP_MODIS with *SNPP*-VIIRS continuity cloud products (CLDPROP_VIIRS), and MYD06 with CLDPROP_VIIRS, respectively. Linear correlation coefficients between the variables on x- and y-axes are given in each plot.



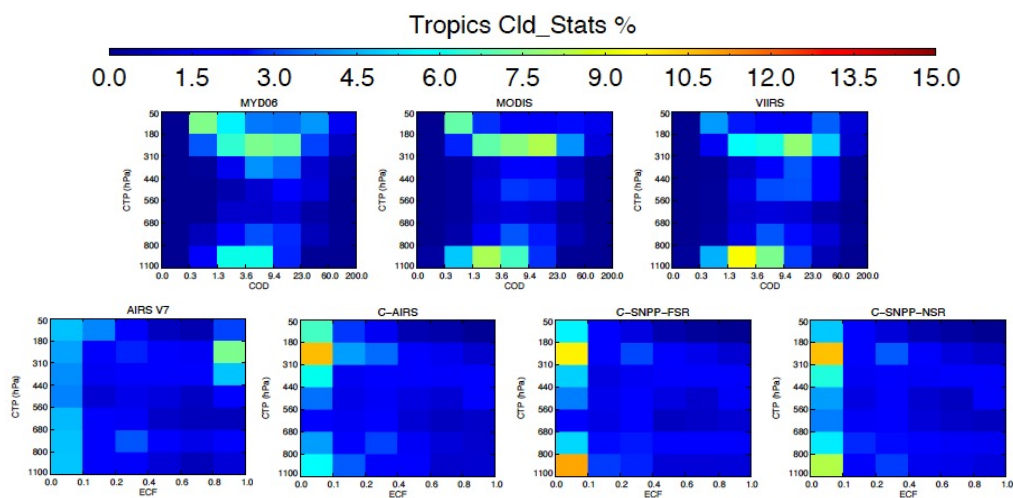
1016
1017
1018
1019
1020
1021

Figure 8. Similar to Fig. 7, except showing comparisons of standard deviation of cloud properties over the sounder FOV, which are calculated using the finer resolution imager observations collocated with the same sounder FOV. All the results are presented on log10 scale. Linear correlation coefficients between the variables on x- and y- axes are given in each plot.

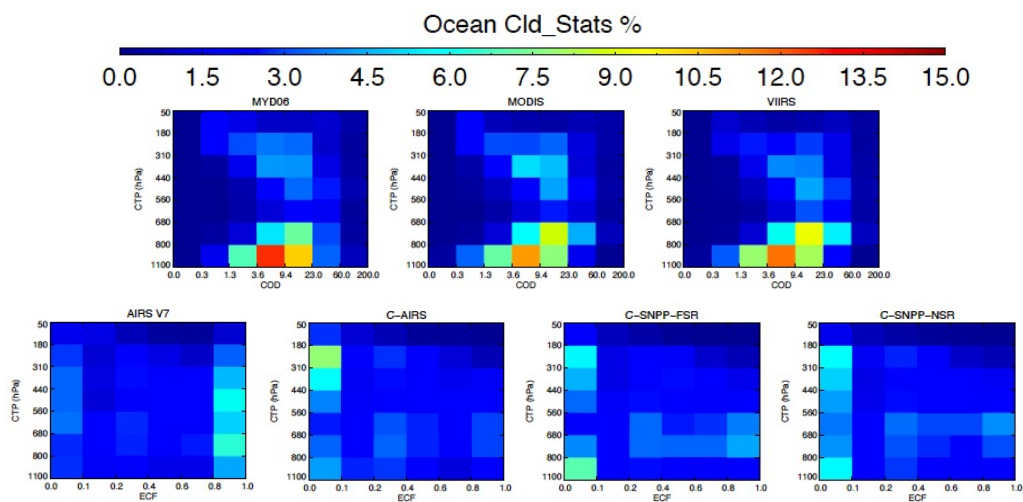


1022
1023
1024
1025
1026
1027

Figure 9. Similar to Figs. 8 and 7, except cloud property skewness over sounder FOV is used in the comparison. Results are shown in linear scale. Linear correlation coefficients between the variables on x- and y-axes are given in each plot.

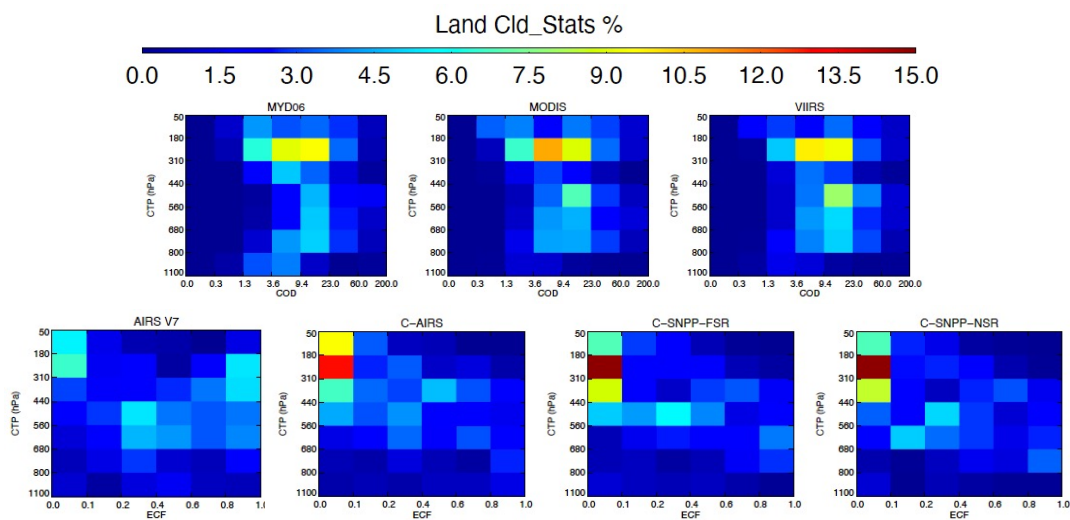


1028
1029 Figure 10. The 2-dimensional histograms calculated using SNOs from the focus days in the
1030 tropics ($30^{\circ}\text{N}\sim 30^{\circ}\text{S}$). The top row shows results for MODIS and VIIRS, for which the ISCCP
1031 type of COD-CTP joint histograms are presented by summarizing the histograms over individual
1032 AIRS and CrIS FOV. Note that no averaging over sounder FOV is taken for this comparison.
1033 From left to right show results of MYD06, *Aqua*-MODIS continuity, and *SNPP*-VIIRS
1034 continuity cloud products. The bottom row shows results for AIRS and CrIS, and joint
1035 distributions are calculated on the imager effective CTP and ECF space. From left to right, data
1036 from AIRS Version 7 (AIRS V7), CLIMCAPS-*Aqua* (C-AIRS), CLIMCAPS-*SNPP* FSR (C-
1037 *SNPP*-FSR), and CLIMCAPS-*SNPP* NSR (C-*SNPP*-NSR) are used in the calculation.
1038
1039

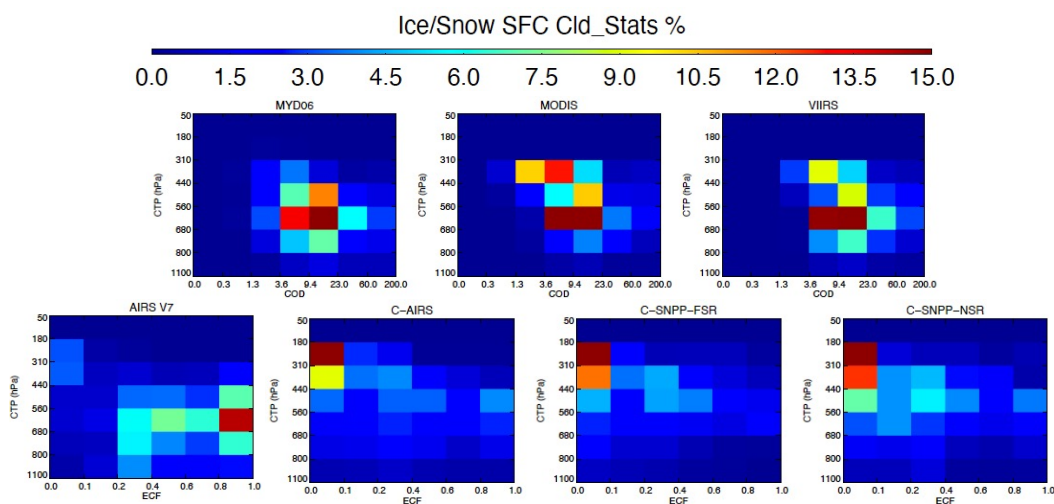


1040
1041
1042
1043
1044

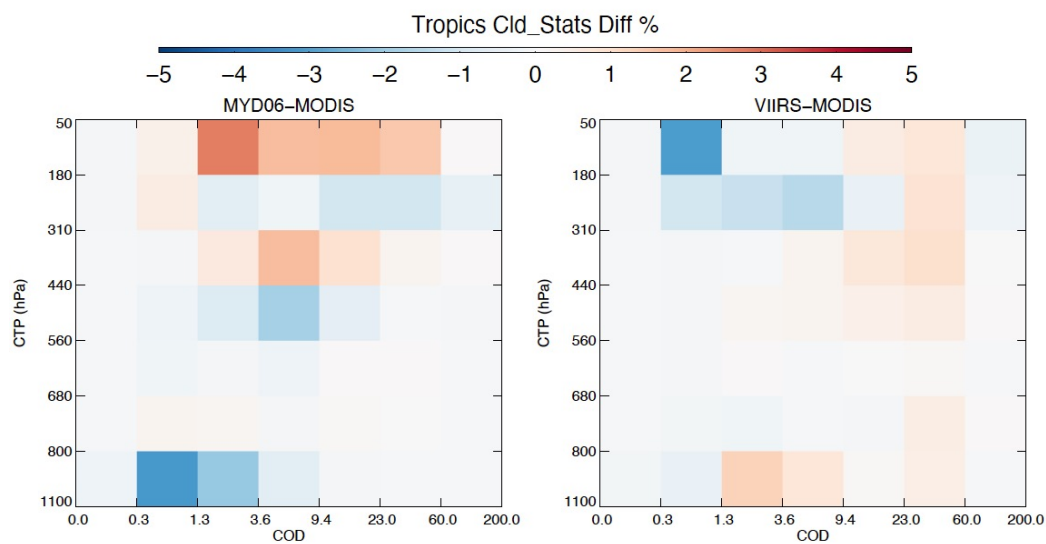
Figure 11. Similar to Fig. 10, except showing results calculated using data over 60°N~60°S ocean. Sounder land fraction < 0.1 is used to determine ocean surfaces.



1045
1046 Figure 12. Similar to Figs. 11 and 10, except showing results calculated using data over
1047 60°N~60°S land. Sounder land fraction > 0.9 is used to determine land surfaces.
1048
1049

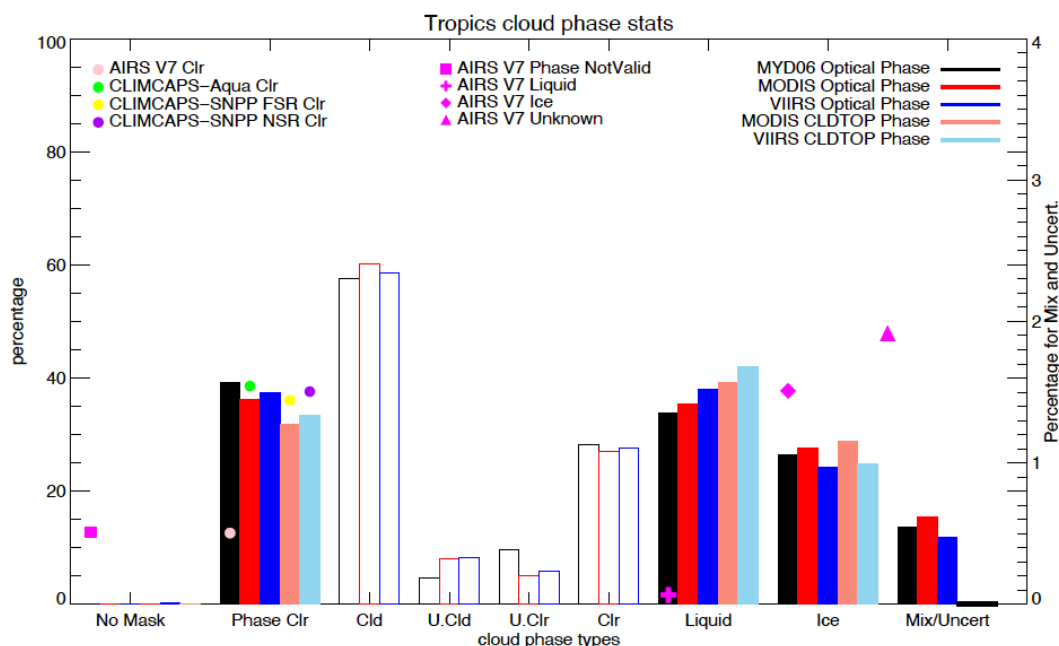


1050
1051 Figure 13. Similar to Fig. 10-12, except showing results calculated using data over snow and ice
1052 covered surfaces. Sounder retrieved surface classes are used to identify cases.
1053
1054
1055



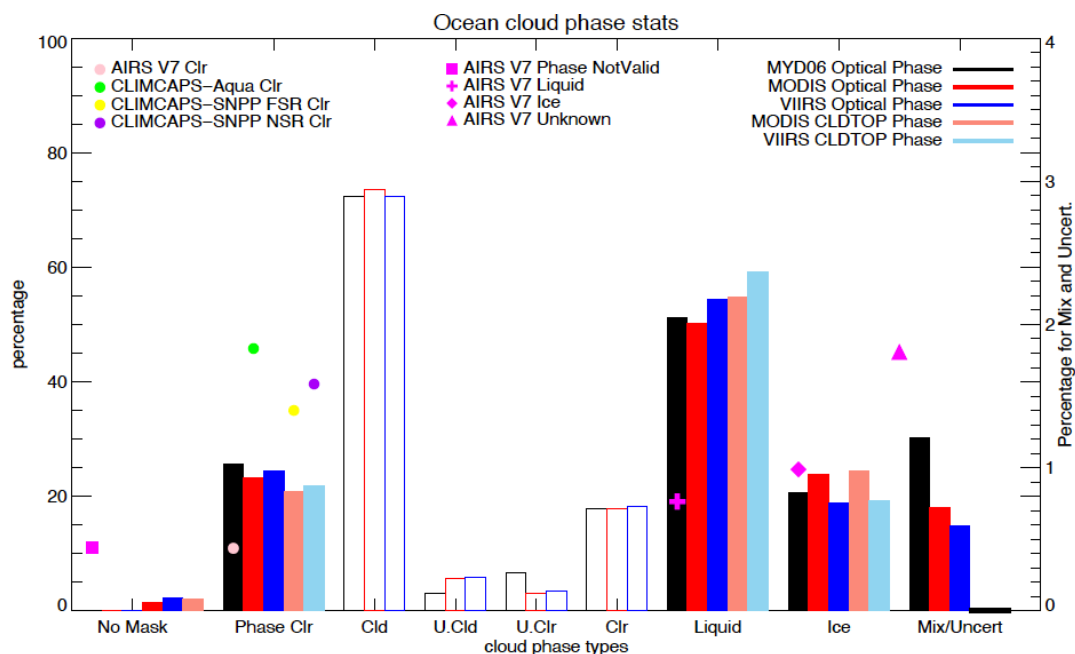
1056
1057
1058
1059
1060
1061
1062

Figure 14. Differences of the imager CTP-COD cloud histograms in the tropics: between the MYD06 and *Aqua*-MODIS continuity products (left), and between the *Aqua*-MODIS and *SNPP*-VIIRS continuity cloud products (right).



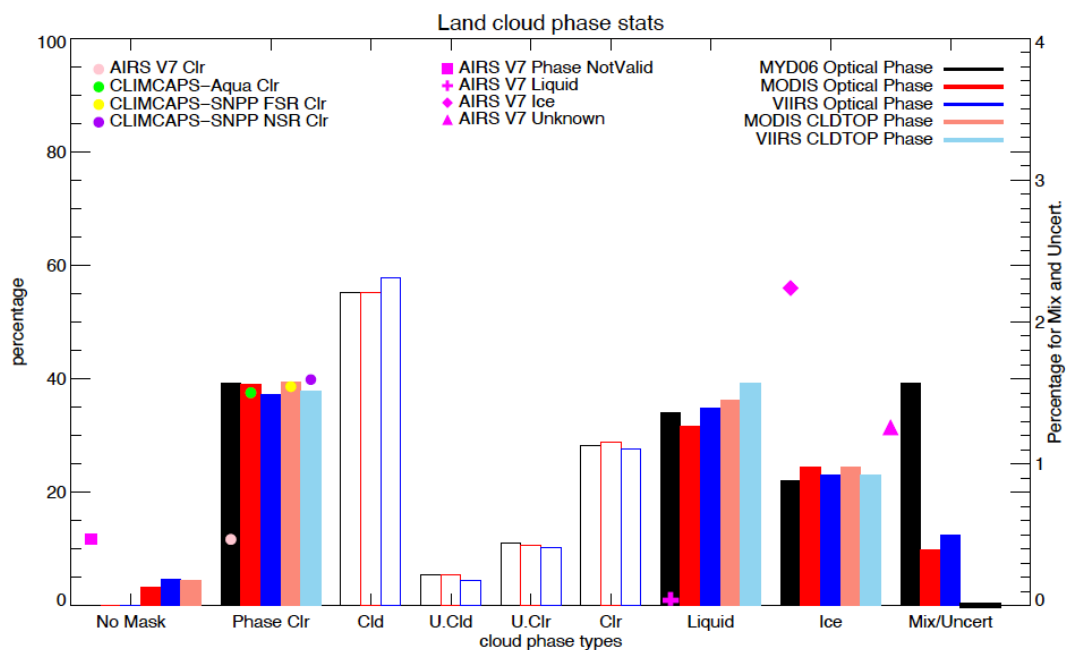
1063
 1064 Figure 15. The histograms of cloud thermodynamic phases (solid color bars) and cloud mask
 1065 (hollow color bars) in the tropics (30°N~30°S) from the imager cloud products calculated using
 1066 retrievals on SNOs from the seven focus days. The frequency of clear sky detected by IR
 1067 sounders using thresholds of ECF < 0.01 is also shown by colored solid circles. AIRS Version 7
 1068 cloud thermodynamic phase is shown by magenta symbols. Color of the bars corresponds with
 1069 different imager cloud retrievals for cloud mask and cloud thermodynamic phase determined in
 1070 the optical property retrieval (Cloud_Phase_Optical_Properties): black for MYD06, red for Aqua
 1071 MODIS continuity products (CLDPROP_MODIS), and blue for SNPP VIIRS continuity
 1072 products (CLDPROP_VIIRS), respectively. Cloud_Phase_Optical_Properties reports flags
 1073 indicating cloud mask not determined for pixel (no mask), clear sky (Phase Clr), liquid water
 1074 cloud (Liquid), ice cloud (ICE), or undetermined phase (Mix/Uncert). Cloud phases reported by
 1075 Cloud_Phase_Cloud_Top_Properties in the MODIS-VIIRS continuity cloud products are also
 1076 evaluated and results are shown with pink (MODIS) and light blue (VIIRS) bars, which shows
 1077 flags indicating cloud free (Phase Clr), water cloud (Liquid), ice cloud (ICE), mixed phase cloud
 1078 or undetermined phase (Mix/Uncert). Note that the Mix/Uncert phase category for imager
 1079 products is shown with the y-axis on the right due to its much smaller frequency of occurrence.
 1080 Cloud mask histograms of Not determined (No Mask), Cloudy (Cld), Uncertain (U. Cld),
 1081 Probably Clear (U. Clr), and Confident Clear (Clr) are shown in the figure following this color
 1082 convention but using hollow bars. For IR sounder clear sky frequency, results from AIRS V7
 1083 (pink), CLIMCAPS-AIRS (green), CLIMCAPS-SNPP FSR (yellow), and CLIMCAPS-SNPP
 1084 NSR (purple) are overlaid on top of the Phase Clr histograms for sounder-imager clear sky
 1085 detection comparison.

1086
 1087
 1088



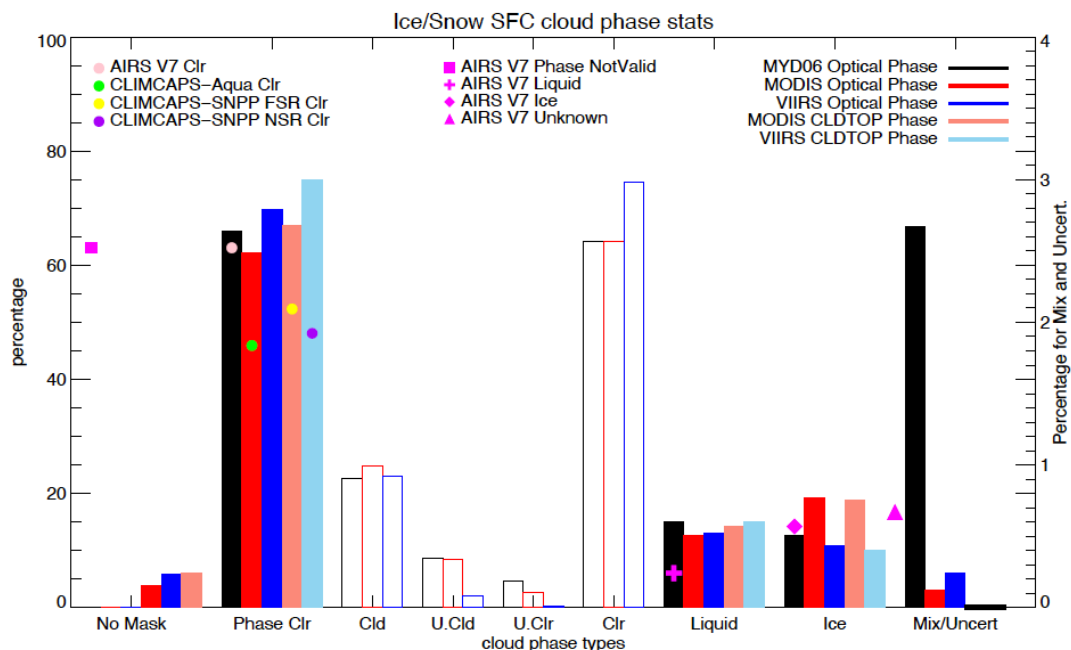
1089
 1090
 1091
 1092
 1093

Figure 16. Similar to Fig. 15, except showing results calculated using data over 60°N~60°S ocean. Souder land fraction < 0.1 is used to determine ocean surfaces.



1094
 1095
 1096
 1097
 1098
 1099

Figure 17. Similar to Figs. 16 and 15, except showing results calculated using data over 60°N~60°S land. Sounder land fraction > 0.9 is used to determine land surfaces.



1100
 1101
 1102
 1103
 1104
 1105

Figure 18. Similar to Figs. 15-17, except showing results calculated using data over snow and ice covered surfaces. Sounder retrieved surface classes are used to identify cases.